Protein functionalized nanocomposite based platform for Cancer Detection

A major project dissertation submitted
in partial fulfillment of the requirement for the degree of

Master of Technology
in
Biomedical Engineering

Submitted by
GURPREET SINGH SAINI
(2K14/BME/07)

Delhi Technological University, Delhi, India

Under the supervision of
Prof. Bansi D. Malhotra

Department of Biotechnology
Delhi Technological University
Delhi-110042, INDIA

DECLARATION

Certified that the project report entitled **"Protein functionalized nanocomposite based platform for Cancer Detection"** submitted by me is in partial fulfilment of the requirement for the award of the degree of Master of Technology in Biomedical Engineering, Delhi Technological University. It is a record of original research work carried out by me under the supervision of **Prof. Bansi. D. Malhotra**, Department of Biotechnology, Delhi Technological University, Delhi.

The matter embodied in this project report is original and has not been submitted for the award of any Degree / Diploma.

Date:

Gurpreet Singh Saini
(2K14/BME/07)
Department of Biotechnology
Delhi Technological University
Delhi-110042.

Certificate

This is to certify that the major project entitled **"Protein functionalized nanocomposite based platform for Cancer Detection"** submitted by **Gurpreet Singh Saini(2K14/BME/07)** in partial fulfillment of the requirement for the award of the degree of Master of Technology in Biomedical Engineering, Delhi Technological University, is an authentic record of the candidate's own work carried out by him under my supervision. The information and data enclosed in this dissertation is original and has not been submitted elsewhere for honouring of any other degree.

Date:

Prof. D. Kumar
Head
Department of Biotechnology
Delhi Technological University
Delhi -110042

Prof. Bansi D. Malhotra
Project Mentor
Department of Biotechnology
Delhi Technological University
Delhi -110042.

ACKNOWLEDGEMENT

First and fore-most I bow down to the divine almighty for providing me inspiration, support and constant strength to achieve this milestone which can add meaning to my life.

This dissertation report would not have been possible without the generous help from many people. First of all, I would like to express my profound sense of reverence of gratitude to my mentor Prof. Bansi D. Malhotra, Department of Biotechnology, Delhi Technological University, for his valuable guidance, congenial discussion, incessant help, calm, endurance, constructive criticism and constant encouragement throughout this investigation right from the imitation of work to the ship shaping of manuscript.

I express my kind regards and gratitude to Prof. D. Kumar (HOD, Department of Biotechnology), and all faculty members for helping in my project.

I am highly indebted to Mr. Saurabh Kumar and Mr. Suveen Kumar (Research Scholar) for their guidance and constant supervision as well as for providing necessary information regarding the instruments and experiments and also for their support in completing the report. I am highly grateful to Ms. Shine Augustine, and Dr. Saurabh Shrivastava for their valuable suggestions and guidance during the entire tenure of my dissertation work.

I would also like to thanks Mr. Chhail Bihari, Mr. Jitendra Singh and Mr. Mukesh Kumar for providing necessary chemicals and maintaining laboratory in good condition.

At last but never the least, words are small trophies to express my deep sense of gratitude and affection to my loving friend and my parents who gave me infinite love to go for this achievement.

Gurpreet Singh Saini

CONTENTS

List of Abbreviations

Ab	Antibodies
AgCl	Silver chloride
BSA	Bovine serum albumin
CE	Counter electrode
CEA	Carcinoembryonic antigen
DI water	De-ionized water
EC	Electrochemical
E_{pa}	Anodic peak potential
E_{pc}	Cathodic peak potential
EDC	N-ethyl-N'-(3-dimethylaminopropyl) carbodiimide
ELISA	Enzyme linked immune sorbent assay
EPD	Electrophoretic deposition
FDG-PET	fluoro-2-deoxy-D-glucose-Positron Emission Tomography
GO	Graphene oxide
I_{pa}	Anodic peak current
I_{pc}	Cathodic peak current
IL	Inter-leukin
ITO	Indium-tin-oxide
$K_3[Fe(CN)_6]$	Potassium ferricyanide
$K_4[Fe(CN)_6]_3H_2O$	Potassium ferrocyanide
LOD	Limit of detection
NHS	N-hydroxysuccinimide
PEDOT	Poly(3,4-ethylenedioxythiophene)
PSS	Polystyrene sulfonate
Pt	Platinum
PVDF	Polyvinylidene fluoride
RGO	Reduced graphene oxide
TEM	Transmission electron microscope
V	Volt

List of table

List of Schemes/Figures

Chapter-1

Abstract

Protein functionalized nanocomposite based platform for cancer detection

Gurpreet Singh Saini

Delhi Technological University, Delhi, India

Email ID.:- gurpreet2619@gmail.com

1. Abstract

This dissertation contains results of the studies relating to fabrication of the label free and, novel nanostructured immunosensor platform (BSA/anti-CEA/PEDOT/RGO/ITO) for efficient detection of a cancer biomarker, carcinoembryonic antigen (CEA). Nanostructured PEDOT/RGO has been synthesized via one step low temperature hydrothermal process and surface modified by covalent immobilization of monoclonal anti-CEA. Structural and morphological characterization of the fabricated electrodes has been carried out using X-ray diffraction (XRD), transmission electron microscopy (TEM) and scanning electron microscopy. The results of the response studies reveal that the BSA/anti-CEA/PEDOT/RGO/ITO immunoelectrode can be used to estimate the CEA with a high sensitivity of 1.8 μA mL ng^{-1}has a wide linear detection range (LDR) of 0.5-15 ng mL^{-1} and limit of detection (LOD) as 0.208 ng mL^{-1}. The biosensing characteristics of the fabricated PEDOT/RGO nanocomposite based immunoelectrode reveal that this platform can be efficiently utilized for the fabrication of point of care (POC) device for cancer monitoring.

Keywords: - PEDOT/RGO, anti-CEA, nanostructured,

Chapter-2

Introduction

2. Introduction

Cancer is a genetic disease that is caused by changes to genes that control the way our cells function, especially how they grow and divide. Genetic changes that cause cancer can be inherited from our parents. They can also arise during a person's lifetime as a result of errors that occur as cells divide or because of damage to DNA caused by certain environmental exposures. Cancer is currently the leading cause for deaths throughout the world. Cancer causes more deaths than combined deaths by coronary heart disease (CHD) or stroke. As per the estimates of the International Agency for Research on Cancer (IARC) Lyon France, the combined global burden of incidence and mortality from 27 major cancers is expected to grow to 21.7 million from the present 14.1 million by 2030. Overall, there were 14.1 million new cases and 8.2 million deaths in 2012. The most commonly diagnosed cancers are lung (1.82 million), breast (1.67 million), and colorectal (1.36 million) and the most common causes of cancer death were lung cancer (1.6 million deaths), liver cancer (745,000 deaths), and stomach cancer (723,000 deaths) globally (Ferley et al., 2015). Therefore, early diagnosis of cancer as well as planning of appropriate treatment is highly desirable. The conventional methods such as immunohistopathology, radioimmuno assays (ELISA), reverse transcriptase polymerase chain reaction (RT-PCR) and fluoro-2-deoxy-D-glucose-Positron Emission Tomography (FDG-PET) currently being used for detection and monitoring of the oral cancer are expensive, labor intensive, time consuming and require considerable volumes of serum/blood (Goldenberg et al., 1978, 1980; Von Kleist et al., 1975; Lai et al., 1996; Zhou et al., 2012; Xu et al., 2006; Flanagan et al., 1998; Nakanishi et al., 2000; Yonemura et al., 2001). Although a number of modification have been used with conventional techniques yet the achieved sensitivity and specificity of these techniques is low and calls for an urgent need for rapid, reliable, specific, and sensitive alternative technique for cancer detection. In this perspective, biosensors have been considered as an attractive, rapid and cost-effective technique for the detection of cancer. Among the various biosensors, electrochemical (EC) biosensors are considered promising bioanalytical devices as they offer high sensitivity, improved detection limit, multianalyte detection, automation, require small sample volume and are not affected by sample turbidity (Rasooly et al., 2006; Tothill et al., 2009; Malhotra et al., 2010, 2015; Wang et al., 1999, 2006; Chen et al., 2011; Feng et al., 2011).

Besides this, they require relatively simple instrumentation that requires low power and can be easily miniaturized thereby imparting portability.

Early diagnosis of tumor biomarkers is critical for treatment of cancer. Some of the important biomarkers in cancer detection are interleukin-8 (IL-8), interleukin-6 (IL-6), interleukin-2α (IL-2α), prostate protein antigen (PPA), carcinoma antigen (CA 125, CA153, CA 199), α-fetoprotein (AFP), p-53, vascular endothelial growth factor (VEGF) and epidermal growth factor receptor (EGFR). Carcinoembryonic antigen (CEA) is one such tumor biomarker known to be associated with colorectal/colon cancer (Wanebo et al., 1978; Moertel et al., 1993; Duffy et al., 2001), lung cancer (Said et al., 1983; Kulpa et al., 2002), ovarian cancer (Engelen et al., 2000; Galanis et al., 2010), gastric cancer (Nakane et al., 1994; Ishigami et al., 2001) and breast cancer (Myers et al., 1978; Hayes et al., 1986) that are responsible for more than half of the deaths caused by cancer (Hirata et al., 2014). The level of CEA in normal subjects is < 3 ng mL^{-1} with cutoff value of 5 ng mL^{-1} whereas in cancer patients the level increases to as high as 24 ng mL^{-1} (Laurence et al., 1972). The performance of an Electrochemical biosensor is known to depend on the physiochemical properties of the material and biomolecules immobilized onto an electrode (Arya and Bhansali 2011; Kumar et al. 2013; Wang 2006). Direct immobilization of antibody onto an electrode surface requires materials with large surface-to-volume ratio, biocompatibility and ease of surface modification (Ali et al. 2013; Arya and Bhansali 2011; Solanki et al. 2011). Nanomaterials have been known to possess novel properties not known in the corresponding bulk materials due to the nanometer dimension. The low dimension imparts these nanomaterials with high surface energy, large number of surface atoms, spatial confinement and reduced imperfections. Owing to the small dimensions, nanomaterials have large surface to volume ratios that imparts larger surface for surface modifications and result in more surface dependent material properties. These distinct properties of nanomaterials provide excellent surface for biomolecules immobilization and high biological activity providing enhanced biosensing characteristics. Conducting polymer (CP) nanocomposites have been extensively used for surface modification in biosensor fabrication (Njagi et al., 2007; Ahuja et al., 2009). The charge-transport properties of CP nanomaterials enable sensitive sensing by tuning the CP characteristics. The surface functional groups of CP nanomaterials can be modified covalently using specific bioreceptors, allowing the immobilization of CP nanomaterials on electrode substrates. Therefore, CPs have been predicted to have enough potential for the development of a

low cost and high performance biosensor materials that offer high permeability biocompatibility, and rapid electron transfer (Istamboulie, Georges, et al., 2010).

PEDOT:PSSor **poly(3,4-ethylenedioxythiophene) polystyrene sulfonate** is a polymer mixture of two ionomers. One of the components made up of sodium polystyrene sulfonate which is a sulfonated polystyrene. Part of the sulfonyl groups are deprotonated and carry a negative charge. The other component poly(3,4-ethylenedioxythiophene) or **PEDOT** is a conjugated polymer and carries positive charges and is based on polythiophene. Together the charged macromolecules form a macromolecular salt. The combination of an especially low oxidation potential and a relatively low band gap (**~ 1.6 eV**) gives PEDOT some unique electrochemical and spectroscopic properties not accessible in other polymers (Jönsson, S. K. M., et al., 2003). Graphene a two dimensional atomic crystal is known to be sensitive to the environment due to its two dimensional structure and surface without bulk. This unique property has led it to be used for sensor applications. Reduced graphene oxide (RGO) has been used to fabricate biosensors (Kumar et al., 2015).

This dissertation contains results of studies relating to the fabrication of nanocomposite PEDOT/RGO based immunosensor based on carcinoembryonic antigen (CEA) for detection of cancer. Efforts have also been made to investigate the structural and electrochemical characterization of anti-CEA immobilized nanocomposite PEDOT/RGO electrode.

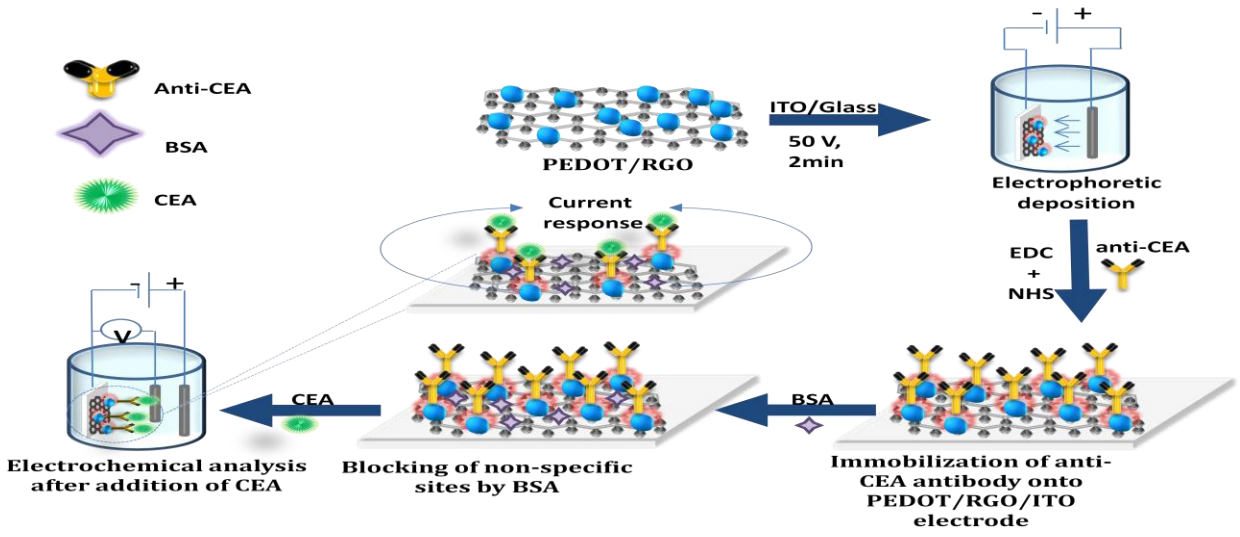

Scheme 1. Fabrication steps of BSA/anti-CEA/PEDOT/RGO/ITO platform for CEA biomarker detection.

Chapter-3

Literature Review

3.1 Cancer

Cancer is defined as abnormal and uncontrolled cell growth due to an accumulation of specific genetic (changes in cell's DNA sequence) and epigenetic (without a change in DNA sequences) defects, which are either environmental or hereditary in origin (Bohunicky et al.,2011). A normal cell undergoes regulated division, differentiation and apoptosis (programmed cell death). When normal cells have lost their division, differentiation and apoptosis they become tumor cells. So, a tumor is the result of abnormal proliferation of cells without differentiation and apoptosis. The unregulated cell growth leads to the formation of a tumor mass that over time becomes independent of normal homeostatic checks and balances (Hanahan et al.,2011). As the cancer progresses, the tumor begins to spread beyond the site of origin and metastasizes to other body organs and systems, making it incurable (Bohunicky et al.,2011). Most cancers are initiated by genetic changes and majority of them are caused by changes in somatic cells and therefore are not transmitted to next generation. About 1% of all cancers is due to genetic changes in germinal cells and is therefore inherited. About 80% of these inherited cancers are dominant in nature. More than 200 distinct forms of cancer exists which include lung, prostate, breast, ovarian, hematologic, skin, and colon cancer, and leukemia etc (Rasooly et al., 2006). Some cancers like stomach and cervical cancer are strongly associated with bacterial and viral infections respectively (Chen et al., 2012). Diagnosing a cancer via cross sectional imaging (CT scan) and biopsy is an expensive and often uncomfortable approach for patients and yield substantial false-negative rates and a limited potential for early diagnosis of disease (Hurt et al., 2008; Mehta et al., 2010). Therefore technologies to recognize and understand the signatures of normal cells and how these become cancerous, promise to provide important insights into the aetiology of cancer that can be useful for early detection, diagnosis, and treatment (Madu et al., 2010).

3.2 Cancer biomarkers

The detection of clinical biomarkers plays a crucial role in the early detection of a cancer, design of individual therapies, and to identify underlying processes involved in the disease (Palma et al., 2012). Biomarkers are chemical substances related with the elevation of malignant tumors which

are found in blood, urine, or body tissues (Henry et al., 2012). They are normally produced directly by the embryonic tissue or neoplasm tissue (Preedy et al., 2015). Biomarkers indicate changes in the expression of a protein that is correlated to risk or progression of a disease or its response to treatment, and that can be measured in tissues or in the blood (Preedy et al., 2015; Hori et al., 2011). As a result, biomarkers can be specific cells, molecules or genes, gene products, enzymes or hormones. An ideal cancer biomarker should have high clinical sensitivity and specificity, quick release in the blood enabling early diagnosis, capability to remain elevated for longer time in the blood, and ability to be assayed quantitatively (Hori et al., 2011; Wu et al., 2015; Gillette et al.,2013). More than 160 types of biomarkers are identified that are being used for the detection of cancer (Kumar et al., 2013). The expression of specific biomarkers and their accurate detection can be helpful in the diagnosis, staging and effective treatment of a cancer at an early stage. Various cancer markers such as are interleukin-8 (IL-8), interleukin-6 (IL-6), interleukin-2α (IL-2α), prostate protein antigen (PPA), carcinoma antigen (CA 125, CA153, CA 199), α-fetoprotein (AFP), p-53, vascular endothelial growth factor (VEGF) and epidermal growth factor receptor (EGFR) are being widely used for diagnosing cancer, but carcinoembryonic antigen (CEA) is known to be a tumor marker associated with colon, lung, ovarian and breast cancer that are responsible for more than half of all cancer deaths each year (Hirata et al., 2014).

3.3 Carcinoembryonic antigen (CEA)

Carcinoembryonic antigen (CEA) belongs to cell surface glycoprotein family that is produced in excess in essentially all human colon carcinomas and in a high proportion of carcinomas at many other sites. The function of this widely used tumor marker and its relevance to malignant transformation is therefore of considerable interest. The overproduction of CEA or related family members in human tumors is an extremely common cellular phenotypic change which has led to the development of extensively used clinical assays. The function(s) and significance to malignant transformation of these antigens have, however, remained completely unknown. CEA is a highly glycosylated cell surface glycoprotein containing approximately 50% carbohydrate with a molecular weight of 200 KDa (Hammarstrom et al., 1999) (protein, 72,800), and is expressed at greatly increased levels in nearly all human colon carcinomas (Shuster et al., 1980).

CEA consists of an amino-terminal domain with a processed leader sequence, three very similar internal domains, and a short 27 amino acid hydrophobic carboxy-terminal domain.

3.4 Conventional methods for detection of CEA

Carcinoembryonic antigens (CEA) described almost five decades ago by Gold and Freedman (Gold et al., 1965) was previously hypothesized to be an oncofetal antigen but is actually expressed in normal adult tissue as well. Over few decades, CEA has been favored as target antigen for primary and metastatic colorectal detection and other carcinomas of epithelial origin (Hammarstrom et al., 1999). Owing to technological advancements various methods for CEA detection have developed over the years ranging from immunohistopathology to Radioimmuno assays (Enzyme linked immune sorbent assay-ELISA) and reverse transcriptase polymerase chain reaction (RT-PCR) to radioactive tracer fluoro-2-deoxy-D-glucose-Positron Emission Tomography (FDG-PET) detection.

1. **Immunohistopathology for CEA detection**

Goldenberg et al reported a 3-step unlabeled antibody immunocytochemical staining method for CEA detection where horseradish peroxidase stain was used. The antibodies used were goat anti-CEA antiserum and rabbit anti-goat I_gG. Tissue specimens from 950 patients were fixed in ethanol and formalin and stained for CEA detection. The immunocytochemical reaction detected CEA concentrations above 0.7 µg/g in ethanol fixed and 3.0-5.0 µg/g in formalin fixed specimens. The CEA concentration values detected by this method are considerably high that indicates low sensitivity of the method (Goldenberg et al., 1978).

Kleist et al used continuous cell line (HT29) from human carcinoma of the colon for synthesizing colon tumor antigen CEA which was detected by immunofluorescence technique. Anti-sera (aCEA) were prepared in rabbits and then the cells were incubated in sheep immunserum against rabbit I_gG with isothiocyanate of Fluorescein (IF). The weaker fluorescence of CEA indicated low sensitivity of the detection method (Kleist et al., 1975).

2. Radioimmuno assays

Goldenberg et al reported a Radioimmuno detection technique for CEA detection in which the prepared hyperimmune goat I_gG against CEA was radio labeled with ^{133}I (Iodine radioactive isotope). A study population of 142 patients was injected with CEA antibody I_gG and scanned using a γ-scintillation camera. The detection limit of this method was 2 cm and any tumor below 2 cm was undetectable which was a major drawback of this method (Goldenberg et al., 1980).

Thomson et al proposed a Radioimmuno detection technique for circulating CEA detection in which purified CEA was radioiodinated by ^{125}I (Iodine radioactive isotope). Goats were immunized with pure CEA to produce anti-CEA antiserum that was incubated with ^{125}I-CEA. The autoradiography results showed a single band identical to pattern obtained upon ordinary immunoelectrophoresis. The group claims to have successfully detected circulating CEA in 35 of the 36 patients with tumor of colonic or rectal origin. The low sensitivity of 2.5 ng of CEA/ml of serum is attributed to the low specific activity of the ^{125}I-CEA (Thomson et al., 1969).

3. Enzyme linked immune sorbent assay (ELISA)

ELISA has been considered as gold standard technique for detection of proteinaceous molecules and has been traditionally employed for tumor antigen, CEA detection (Lai et al., 1996). Various modified ELISA techniques using gold nanoparticles have been used to further improve the sensitivity (Zhou et al., 2012). ELISA is a time consuming, complex and expensive detection method.

4. Real time reverse transcription - PCR (RT-PCR)

Dong et al employed a real time reverse transcription PCR for determination of CEA mRNA molecules in peripheral blood of 95 colorectal carcinoma (CRC) patients. The sensitivity of the method achieved was 2 copies per tube that were high enough to determine very low levels of CEA in peripheral blood (Dong et al., 2006).

Nakanishi et al used a modified RT fluorescence PCR system (Lightcycler) owing to the lack of quantitative assessment of free cancer cells and the length of time before completion in conventional RT-PCR. This method used hybridization probes as flurophores to detect CEA in peritoneal washes of 109 gastric cancer patients. The group claimed to reproducibly quantitate 10 to 10^6 CEA-expressing colon carcinoma cells per 10^7 peripheral blood leukocytes using this method (Nakanishi et al., 2000).

Yonemura et al employed RT-PCR coupled with conventional cytological assay for determination of CEA mRNA in peritoneal washes of 230 patients of gastric cancer. The sensitivity achieved by combining RT-PCR with cytological assay resulted in higher sensitivity over the conventional cytological assay alone (Yonemura et al., 2001).

5. FDG-Positron Emission Tomography (FDG-PET)

Positron Emission Tomography (PET) is a functional imaging technique relying on physiological changes or metabolic functions for the detection of disease.Fluoro-2-deoxy-D-glucose (FDG) is a radioactive glucose analog used in medical imaging modality PET. The increased glucose metabolism of tumor cells is the base for using FDG-PET in oncology which makes it an important tool for quantitative analysis of malignant tumors. PET has also been employed to distinguish recurrent tumors from post therapeutic changes. Flanagan et al used FDG-PET for investigating unexplained elevation of plasma CEA levels in 22 colorectal cancer patients post colorectal surgery. PET was more sensitive than conventional imaging methods with a positive predictive value of 89% (15 out of 17) in CRC patients (Flanagan et al., 1998).

Liu et al investigated recurrent serum breast cancer tumor CEA using FDG-PET in 30 breast cancer patients. The whole body FDG-PET revealed recurrent breast cancer tumor in 28 of the patients and accurately detected 35/38 tumor sites in 25/28 patients with recurrence with 90% sensitivity (Liu et al., 2002).

These conventional techniques hold advantage in providing low detection limits but are complex, time consuming and expensive. The requirement of trained personnel and expensive equipments as in case of FDG-PET is another major disadvantage of these techniques. They are not rapid and the diagnosis period ranges from few hours to few days making them laborious and time consuming. The success of these techniques has been marred by low sensitivity and specificity. Although a number of groups have modified the fundamental techniques for obtaining better results, like modified fluorescence RT-PCR, combining conventional cytology with RT-PCR, Radioimmuno assays yet the achieved sensitivity and specificity of these techniques is low and calls for an urgent need for rapid, reliable, specific, and sensitive alternative technique for cancer detection.

3.5 Biosensor

Biosensor is a bioanalytical device, which converts a biological response into a measureable signal. Biosensor is used to estimate the concentration of desired substances and other parameters of biological interest. As per IUPAC directives "A biosensor is a self-contained integrated electronic device capable of providing specific quantitative or semi- quantitative analytical information using a biological recognition element which is retained in direct spatial contact with a transduction element" (Gerard et al., 2002).Biosensors may be classified into six basic groups, based on the method of signal transduction: optical, mass, micromechanical, electrochemical, magnetic, and thermal sensors. Among the various biosensors, electrochemical biosensors have received special attention as they allow high sensitivity, lower detection limits, automation, inexpensive testing, and development of disposable devices and methodologies capable of working with very small sample volumes (Malhotra et al., 2015).

3.6 Components of Biosensor

A standard biosensor consists of three major components that are a (i) bio-recognition element such as antibody, DNA, enzyme etc., for selective recognition of an analyte also known as bio-receptor, (ii) an immobilization matrix for the immobilization of a recognition biomolecule and (iii) a transducer for conversion of biochemical response into a measurable signal. Bio-receptor and transducer are together referred to as a biosensing membrane.

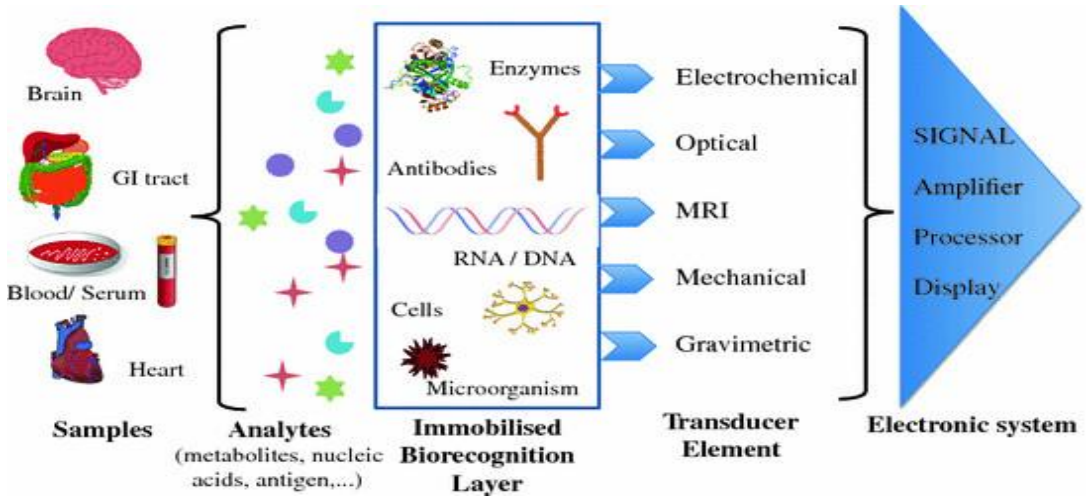

Scheme 2. Components of biosensor

3.6.1 Biomolecular recognition element

Biomolecular recognition element i.e., bioreceptor is a biomolecule or molecular assembly that has the capability of recognizing a target/substrate i.e. an analyte. The most commonly used bioreceptors in biosensors are enzymes, antibodies, and DNA or whole cells. These bio molecular recognition elements having ability to recognize biomarkers secreted in body fluids such as blood, saliva, urine, sweat etc. Among these, blood is one of the prominent body fluid which is commonly used for detection of biomarkers. More than 160 types of biomarkers are identified that are being used for the detection of cancer (Kumar et al., 2013).Various cancer markers such as are interleukin-8 (IL-8), interleukin-6 (IL-6), interleukin-2α (IL-2α), prostate protein antigen (PPA), carcinoma antigen (CA 125, CA153, CA 199), α-fetoprotein (AFP), p-53, vascular endothelial growth factor (VEGF) and epidermal growth factor receptor (EGFR) are being widely used for diagnosing cancer. Carcinoembryonic antigen (CEA) is a known tumor biomarker associated with colon, lung, ovarian and breast cancer. CEA is a highly glycosylated cell surface glycoprotein containing approximately 50% carbohydrate with a molecular weight of 200 KDa (Hammarstrom et al., 1999) (protein, 72,800), and is expressed at greatly increased levels in nearly all human colon carcinomas (Shuster et al., 1980).CEA consists of an amino-terminal domain with a processed leader sequence, three very similar internal domains, and a short 27 amino acid hydrophobic carboxy-terminal domain.

Cancer site	**References**
Colorectal/Colon cancer	Wanebo et al., 1978; Moertel et al., 1993; Duffy et al., 2001
Lung cancer	Said et al., 1983; Kulpa et al., 2002
Ovarian cancer	Engelen et al., 2000; Galanis et al., 2010
Gastric cancer	Nakane et al., 1994; Ishigami et al., 2001
Breast cancer	Myers et al., 1978; Hayes et al., 1986

Table 1. Various cancers with CEA as common biomarker

3.6.2 Nanostructure immobilization matrix

A matrix can be utilized for immobilization or integration of desired biomolecules at the transducer surface and efficiently maintain the functionality of the biomolecules and at the same time provide accessibility towards the target analyte and an intimate contact with the transducer surface. Chemical properties of immobilizing matrix decide the immobilization method and the operational stability of a biosensor. For a preferred immobilizing matrix it should be resistant to a wide range of physiological pH, temperature, ionic strength and chemical composition. Among the various immobilizing matrices, nanostructured immobilization matrices are receiving a great deal of attention owing to their exceptional optical and electronic properties. Nanomaterials are materials with atleast one dimension in the range of 1 -100 nm scale. Nanomaterials of different shapes, sizes and composition have been developed with a view to cater to specific research needs (Poole et al., 2003). Nanomaterials structures are classified as zero dimensional (clusters), one dimensional (nanofibers, rods, wires, tubes), two dimensional (films, plates, networks) and three dimensional (scaffolds) structures. Nanotubes, dendrimers, quantum dots and fullerenes are the most common type of nanomaterials (Pokropivny et al., 2007). The distinct novel properties at nanoscale are due to increased surface area and new quantum effects. The increased surface area to volume ratio lends greater chemical reactivity than their bulk forms. Advancement in nanomaterials has focused research in developing nanostructures with controlled morphologies. The large surface area, high thermal and mechanical stability, abundant functional groups and biocompatibility of nanomaterials makes them ideal candidate for the fabrication of a biosensor.

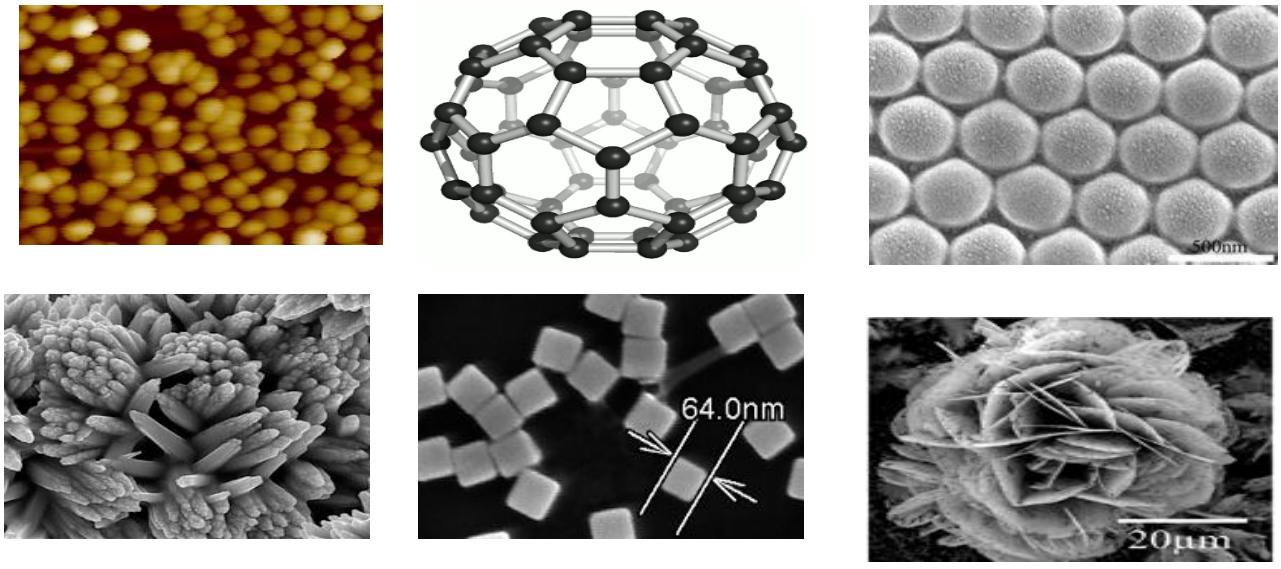

Figure 1.Various Nanomaterial morphologies (Algarasi et al Anal. Chem. 2002)

3.6.2.1. Properties of nanomaterials

Nanomaterials have been known to possess novel properties not known in the corresponding bulk materials due to the nanometer dimension. The low dimension imparts these nanomaterials with high surface energy, large number of surface atoms, spatial confinement and reduced imperfections. Owing to the small dimensions, nanomaterials have large surface to volume ratios that imparts larger surface for reactions and result in more surface dependent material properties. For example, metallic nanoparticles act as active catalyst. The quantum effects of the nanomaterials are due to their spatial confinements. The novel electronic and optical properties of nanomaterials distinct from the bulk material can be brought about by modification in their energy band structure and charge carrier density. For example, quantum dots and quantum wires based light emitting diodes (LEDs) hold promise for future optoelectronics. The increased perfections in the nanomaterials attributed to the self purification (reducing impurities and intrinsic material defects) process enhance their properties. For example, the mechanical properties of nanomaterials are enhanced than their bulk counterparts.

1. **Electrical**

The electrical properties of nanomaterials focus attention on electrical conductivity of nanotubes and nanocomposite and the photoconductivity of nanorods. The electrical conductivity of nanomaterials an attribute of their size is complex due to varied conductivity mechanisms. These mechanisms are grouped into these following categories: Surface scattering, quantized conduction, coulomb charging and tunneling, widening of band gap and change of microstructures. Apart from the above mechanisms, reducing imperfections, structural defects and dislocations improve the electrical conductivity of nanomaterials and nanostructures (G. Cao Nanostructures and nanomaterials 2004).

Voisin et al investigated the conduction electron energy exchanges in Au and Ag nanoparticles of size ranging from 2 to 26 nm. The group used a femtosecond pump-probe technique to probe the internal thermalization dynamics of photo excited electrons. The measurements by the probe reflected the results of theoretical model based on bulk metal electron kinetics and band-structure modeling. This technique successfully observed increased efficiency of the electron-electron interactions or electron-electron energy exchanges ascribed to the size behavior, i.e., with size

reduction in nanomaterials the electrical conductivity improves and is better than that in the bulk metal (Voisin et al., 2003).

Schmid et al reported a novel synthesis and organization technique of Au nanoparticles in 1-3 dimensions to exploit the electrical conductivity of nanomaterials. The molecular assemblies at various dimensions of nanometer scale demonstrated novel and enhanced electrical properties as a result of coulomb charging and electron transfer. This technique effectively utilizes the electrical transport property of nanomaterials which otherwise is absent in the corresponding bulk material (Schmid et al., 2005)

2. Optical

Nanomaterials have known to show distinct novel optical properties, owing to reduction in size than their bulk counterparts. These prominent optical properties have found applications in solar cells, imaging, laser sensor, tumor detection, optical detector, photocatalysis and biomedicine. The novel optical properties in the nanomaterials ascribed to reduction in size is due to increased energy level spacing or quantum confinements arising from spatial confinement of electrons and holes and formation of electric dipoles and discrete electronic energy level in nanomaterials. This phenomenon happens when the size of a nanocrystal is smaller than the de Broglie wavelength. Another phenomenon that takes place due to size reduction is surface Plasmon resonance that is generated when the size of the metal nanocrystals is smaller than the wavelength of incident radiation (G. Cao Nanostructures and nanomaterials 2004). Apart from the size and shape, these optical properties are due to surface characteristics, doping and contact with the immediate environment (Alagarasi, A. "Introduction to nanomaterials." 2011).

Elliman et al observed optical emission from erbium doped silicon nanowires. The silicon nanowires were homegrown on silicon wafers with palladium as catalyst and doped with erbium. These nanowires were irradiated with a light of 480 nm wavelength from Ar-ion laser for analyzing luminescence spectra. The photoluminescence spectrum from nanowires was compared with that of bulk silicon. The group reported prominent photoluminescence (PL) spectra for the nanowires which increased with increasing implanted fluencies as opposed to thermal quenching in the bulk silica which showed initial increased Spectrum that dropped with further increase in the fluencies (Elliman et al., 2008)

Ronning et al observed optical emission from Mn doped ZnO nanobelts. The ZnO nanobelts were developed on silicon by thermal evaporation of the ZnO powder 1350℃ and later doped with Mn^{+} ions. He–Cd laser was used for photoluminescence (PL) investigations. The group reported high quality of PL spectra of the Mn doped ZnO nanobelts as compared to bulk ZnO films (Ronning et al., 2004).

3. Magnetic

One aspect of nanomaterials is their magnetic property, attributed to surface atoms, that is not known in a number of bulk materials. For example, gold and platinum are non-magnetic in bulk form but tend to show magnetic behavior in nanometer size. The Au and Pt nanoparticles have been reported to be magnetic. Ferromagnetic particles tend to switch polarization and become paramagnetic when reduced to nanometer size and are often referred to super paramagnetic particles. The critical estimated size for super paramagnetic behavior in particles is 15 nm and was reported around 1954 in nickel particles dispersed in silica matrix (Heukelom et al., 1954). This magnetic property of nanoparticles has been exploited for biomedical applications such as hyperthermia (increasing body temperature), drug targeting/drug delivery, Nuclear Magnetic Resonance (NMR) imaging, magnetorelaxometry and with a future anticipated application in tumor detection and radiotherapy (Tartaj et al., 2003).

Gao et al reported improved magnetism in magnetite (Fe_3O_4) nanoparticles synthesized by earlier reported co-precipitation method. The earlier reported iron oxide nanoparticles had low magnetic property due to formation of a thin layer of α- FeOOH which the group converted to γ-Fe_2O_3 which resulted in better stability and higher magnetism. The magnetite nanoparticles tend to show more magnetism than the previously reported iron oxide nanoparticles and the bulk material (Gao et al., 2008).

Wu et al synthesized maghemite (γ-Fe_2O_3) short nanotubes (SNTs) by hydrothermal method. The SEM and TEM analysis confirmed the capsule like tubular morphology of the nanotubes. These maghemite nanotubes are reported to have higher stability and magnetism and are ferromagnetic in room temperature. These SNTs have potential applications in biotechnology, biomedicine and spin electronics (Wu et al., 2010).

4. Mechanical

Nanomaterials have reported increased mechanical properties than the bulk materials. Mostly one dimensional nanostructures have been investigated as it is reported that the mechanical properties increase with decreasing size. The most common nanostructures reported are nanowires or nanorods. The mechanical strength of nanostructures (whiskers) has been demonstrated as early as 1952 by Herring and Galt (Herring et al., 1952). The mechanical strength of whiskers is appreciated only below 10 microns. The increased mechanical strength in nanostructures has been ascribed to two mechanisms that are increased internal perfections and less surface defects at nanometer scale. The smaller cross-section area in nanowires reduces the probability of imperfections such as impurity precipitates and dislocations usually found in the bulk material (Lyuttsau et al., 1966). Usually imperfections are introduced in bulk materials to accommodate stress produced during their synthesis and processing which is not found in nanomaterials. Another mechanism is the less surface defects in nanomaterials. Electron microscopy revealed defect free surface morphology of whiskers with diameter below 10 microns and irregular growth steps in whiskers with diameter above 10 microns (A. Nohara et al., 1982)

Wang et al investigated the mechanical properties of carbon nanotubes synthesized by arc-discharge technique. The group synthesized defect free multiwalled carbon nanotubes (MWCNTs) with 5-50 nm diameter and 1-20 μm length. The bending modulus of the CNTs was reported to be 1.2 TPa which is as strong as diamond for nanotubes with 8 nm diameter and decreased to 0.2 TPa as the diameter was increased to 30 nm (Wang et al., 2001)

Zeng et al prepared PA1010 (nylon 1010) and multiwalled carbon nanotubes (MWCNTs) composites via in situ polymerization of carboxylic acid functionalized MWCNTs. The mechanical tensile tests and dynamic mechanical analysis (DMA) were performed to evaluate the mechanical properties of the composite. It was reported that the Young modulus increased on increasing the MWCNT content and elongation at break decreased on increasing the MWCNT content in the composite. This mechanical strength in the composite is attributed to the presence of the MWCNT (Zeng et al., 2006)

5. Catalytic

Catalysis forms an important part of any industrial process. Over the years homogeneous catalysis has been used as it is effective and selective. The limited thermal stability and difficulty in removing the catalyst from the reaction media has focused attention on heterogeneous catalysis that eases the removal of catalyst and possibility of performing reaction at higher temperatures. The search for heterogeneous catalyst has opened avenues for use of transition metal nanoparticles that are selective and efficient as they mimic metal surface activation at nanoscale in heterogeneous catalysis. The sizes of the nanoparticles can vary but the most effective catalysts are the ones in the range of few nanometers. Nanoparticles can themselves participate as catalysts or can be fixated on a matrix such as silicon, polymer, and dendrimers for assisting in heterogeneous catalysis (Astruc, Didier, ed. *Nanoparticles and catalysis*. Vol. 1.Weinheim: Wiley-VCH, 2008).

Tana et al investigated the catalytic properties of ceria nanowires, nanorods and nanoparticles. Hydrothermal process was used to synthesized CeO_2 nanowires and nanorods. To check the catalytic activity of the ceria nanostructures, Carbon monoxide (CO) oxidation in a continuous flow fixed-bed reactor was performed. The highest catalytic activity for CO oxidation was shown by nanowires as they expose a large reactive planes (1 1 0) than the nanorods and nanoparticles. Such large surface area for catalysis is only possible with nanomaterials and is not observed in bulk materials (Tana et al., 2009)

Che et al synthesized monodispersed carbon nanotubes by chemical vapor deposition. These 200 nm diameter CNTs have been filled with electrocatalytic nanoparticles such as Pt, Ru, Pt/Ru. The catalytic activity of nanoparticle filled CNTs was evaluated by electrocatalysing O_2 reduction, methanol oxidation and gas phase catalysis of hydrocarbons. The group reported ~20 times higher current density of methanol oxidation at carbon/Pt nanoclusters membrane than at bulk Pt electrodes. The enhanced current density is ascribed to high surface area and electrocatalytic activity of nanoparticles in the CNTs. The high catalytic activity of these CNTs for gas-phase hydrocarbons open up avenue for advanced fuel cell development (Che et al., 1999).

3.6.2.2. Classification and Application of nanomaterials

Nanomaterials structures are classified as zero dimensional (clusters), one dimensional (nanofibers, rods, wires, tubes), two dimensional (films, plates, networks) and three dimensional (scaffolds) structures. Nanotubes, dendrimers, quantum dots and fullerenes are the most common type of nanomaterials. Advancement in nanomaterials has focused research in develop nanostructures with controlled morphologies.

Metal Nanoclusters (MNCs) (Ag, Au, and Pt) are nano platforms or nano structures with few atoms to some thousands of atoms. They have been preferred over the bulk nanoparticles and small nanoparticles for their fluorescence property at Fermi wavelength due to quantum confinement (Jin et al., 2010). At this size metal nanoclusters have been found to possess distinct optical, electronic, and chemical properties as compared to their bulk counterparts. They have emerged as novel optical probes for biosensors due to their tunable fluorescence and good biocompatibility (Feng et al., 2015). Carbon nanofibers are cylindrical carbon based nanomaterials with stacked cones, cups, or plates shaped graphene layers. The length of these nanofibers is in the order of micrometers, while their diameter varies between some tens of nanometers up to ~200 nm. The entire surface area of carbon nanofibers can be activated making it easily functionalized for use in developing novel nanomaterials based biosensor. It is well known that decreasing the diameter of carbon nanofibers elicits positive physicochemical characteristics (Vamvakaki et al., 2006). The advances in portable biosensor development have focused research on bioelectronic detection using one dimensional carbon nanotubes (CNTs) and conducting polymer based nano wires. These nanostructures have high surface to volume ratio offering real-time, sensitive and multiassay bioelectronic detection. Carbon Nanotubes are basically of two types- Single walled carbon nanotube (SWCNT) which is a single rolled up graphite sheet and Multi walled carbon nanotube (MWCNT) which is an array of concentric graphite sheets. The ease of modification, processing electronic conductivity of carbon nanotubes makes them an important material for development of biosensors (Wang et al., 2005). Among other 1-D nanostructures, nanorods have gained much attention due to their innate potential for electronic and photonic application in real time biosensing. They are mostly synthesized from metals and semiconducting materials with standard aspect ratios ranging from 3-5 (Li et al., 2005). Mostly ZnO nanorods and gold nanorods have been used in biosensor

development. Nanofilms are nanostructured layer-by-layer (LbL) films that form conjugates with biomolecules for sensing application. These layer-by-layer structures and other 1-D nanostructures such as CNTs, nanorods, nanofibers, etc have been extensively used for sensor development (Siqueira et al., 2014). Nanofilms have emerged as a suitable candidate for multiassay lab on chip sensors. Apart from Nanofilms, another 2-D nanostructure that finds use in biosensor development is nanoplate. Nanoplates are synthesized similarly to nanoparticles but by controlling the morphology in the form of a nanoplate (Zhang et al., 2011). 3-D nanostructures are generally created by stacking 2-D structures. The 2-D structures are printed on top of each other to get a resultant 3-D nanostructure. 3-D nanostructures such as dendrimers (metal) are being used in biosensor development for biomolecules immobilization (Li et al., 2010). These 3-D nanostructures are of particular interest due to their photonic, electronic and biomedical applications.

Depending upon the nature of the materials and their unique properties, nanomaterials can be categorized as metallic nanoparticle (gold, silver, iron oxide etc), carbon nanomaterials (graphene, carbon nanotube etc) and polymeric nanomaterials (polyanilinine, PEDOT: PSS fibers etc). These nanomaterials have shown huge potential in biotechnology, biomedical, engineering, radiotherapy and biomedicine.

1. Metallic Nanoparticles

The term metal nanoparticle is used to describe nanosized metals with dimensions (length, width or thickness) within the size range 1-100 nm. Michael Faraday recognized the existence of metallic nanoparticles in solution as early as 1857 (Faraday, M. 1857) and Mie gave the quantitative explanation of their color in 1908 (Mie et al., 1908). The distinct uniqueness of metallic nanoparticle is large surface-area-to-volume ratio as compared to the bulk equivalents, large surface energies, specific electronic structure provided by transition between molecular and metallic states, Surface Plasmon resonance, quantum confinement, presence of a large number of "dangling bonds" and low-coordination sites such as corners and edges, specific chemical properties and the ability to store excess electrons (G. Cao Nanostructures and nanomaterials 2004).Metallic nanoparticles (gold, silver, iron) with distinct properties have intrigued the scientific community for over a century and have found applications in biotechnology,

biomedicine and engineering. This increased focus on metallic nanoparticles is attributed to their prospective applications in nanotechnology. Nowadays these nanoparticles are either synthesized directly from solutions or modified with various chemical functional groups that allow conjugation with antibodies, ligands, and drugs of interest and consequently opening a broad spectrum of potential applications in biotechnology, preconcentration of target analytes, gene and drug delivery vehicles for a targeted drug delivery, magnetic separation, and more notably diagnostic imaging. The metallic nanoparticles play an important role in diagnostic imaging. Various imaging modalities such as Magnetic Resonance Imaging (MRI), Computed Tomography (CT), Positron Emission Tomography (PET), ultrasound, Surface Enhanced Raman Spectroscopy (SERS) and optical imaging require contrast agents (nanoparticulated) to clearly identify the disease state. Metallic nanoparticles such as magnetic (Iron oxide) nanoparticles (Fe_3O_4), gold and silver nanoparticles have been proposed to be used as contrast agents in these imaging modalities because of their distinctive physiochemical properties (Mody et al., 2010).

2. Carbon Nanomaterial:

Carbon is the sixth most abundant material on earth in the form of a number of allotropes with various distinct properties. It is a good conductor as graphite, polymer as hydrocarbons and wide gap semiconductor as diamond (G. Cao Nanostructures and nanomaterials 2004). Carbon nanomaterials have a distinctive place in nanoscience attributed to their exceptional electrical, thermal, chemical and mechanical properties and have found application in areas diverse as composite materials, energy storage and conversion, sensors, drug delivery, field emission devices and nanoscale electronic components. CNMs composed entirely of sp2 bonded carbon, which are found in all dimensionalities including zero-dimensional fullerenes, one-dimensional carbon nanotubes (CNTs), and two-dimensional graphene.

3. Fullerenes

Carbon fullerenes are 60 carbon atom containing molecule, each placed at vertices at equal distance from each other with an icosahedral symmetry. Carbon fullerenes with atoms more than 60 and different geometric structures are also known such as C_{70}, C_{76}, $C_{78,}$ C_{80} (Kroto, Harold W., et al., 1985). Fullerenes have promising potential in environmental sensing and biomolecular

applications as they can act both as a redox catalysts and mediators in electrochemical analysis (Sherigara et al., 2003).

4. Carbon Nanotubes

Carbon nanotubes (CNTs) are one dimensional carbon based nanostructure with unique electrical and mechanical properties. CNTs are normally a graphene sheet rolled into a tube, further classified as per the orientation of axis as *n* and *m* type. CNTs can be classified into Single walled CNTs (SWCNTs), Double walled CNTs (DWCNTs) and Multi Walled CNTs (MWCNTs) depending on the number of carbon layers on the side walls of the tube (Flahaut, Emmanuel, et al., 2003).

Since the synthesis of CNTs some 20 years ago, a number of applications have been demonstrated such as transparent electrodes for organic light-emitting diodes (OLEDs), lithium-ion batteries, supercapacitors, and CNT-based electronic components such as field-effect transistors (FETs). CNTs have been employed in catalysis and sensing as well as filters and mechanical and biomedical applications (Schnorr et al., 2011).

Gheith et al prepared layer-by-layer (LBL) films of Single walled carbon nanotubes (SWCNTs) to study the possibility of electrically stimulating neuronal NG108-15 neuroblastoma/glioma hybrid cells by these electrically conductive LBL SWNTs Films. Voltage/patch clamp technique was used for electrophysiological measurements where cells were voltage clamped. The voltage pulses through the LBL film helps in recording current flow through the cells and clearly indicates the neuronal cell stimulation. This experiment opens avenues for further research in artificial neuronal cell stimulation via LBL-SWCNT film for medical applications (Gheith et al., 2006).

Novak et al developed thin film transistors of Single walled CNTs as a senor for detecting chemical nerve agent such as dimethyl methylphosphonate (DMMP) a stimulant for the nerve agent sarin. These CNT sensors are quite sensitive and can detect DMMP at low concentration levels such as sub-ppb concentration. They are selective enough to avoid interfering signals from hydrocarbon vapors and humidity. These sensors have shown a promising potential for electronic detection of other chemical warfare agents as well (Novak et al., 2003).

Li et al fabricated a gas sensor of single walled CNT on an interdigitated electrode (IDE) for detection of gas and organic vapor at room temperature. The linear range of sensor is sub ppm to hundreds of ppm and limit of detection is 44 ppb and 262 ppb for NO_2 and nitrotoluene (Li et al., 2003).

5. Graphene

The first two-dimensional (2D) atomic crystal, graphene has been the focus of research due to its unique properties such as mechanical strength, elasticity, high electrical and thermal conductivity. Graphene is known to possess characteristics that have exceeded the theoretical limits of any other known material such as room-temperature mobility of 2.5 x 10^5 cm^2 V^{-1} s^{-1}, Young's modulus of 1 TPa, intrinsic strength of 130 GPa (Lee et al., 2008), high thermal conductivity above 3000 W mK^{-1} (Balandin et al., 2011), optical absorption ($\pi\alpha$) of 2.3 %, impermeability to gases, high electric current sustainability and readily chemically functionalization. One advantage of using graphene is the ease of tuning the morphology to obtain various shapes, dimensions and quality for various functions. Based on functions graphene is categorized as 1) graphene or reduced graphene oxide flakes for composite materials, conductive paints, and so on; 2) planar graphene for lower-performance active and non-active devices; and 3) planar graphene for high-performance electronic devices.

Graphene is being used as a transparent conductive coating for touch screens, organic light emitting diodes (OLED), electronic paper and other flexible electronics due to low sheet resistance (~ 30 Ω) and high transmittance (~ 90%) apart from the high mechanical flexibility and chemical durability it provides (Bae et al., 2010). Graphene is known to be sensitive to the environment due to its two dimensional structure and surface without bulk. This unique property has led it to be used for sensor applications for measuring magnetic field to DNA sequencing and monitoring velocity of surrounding liquid to strain gauges. The working range of graphene for sensing application is enhanced significantly as it can be stretched by 20%. A number of biosensors have been fabricated using graphene.

Wang et al used CdS nanocrystals modified single layer of reduced graphene for detection of glucose. This graphene based glucose sensor showed a very low detection limit of 0.7 mM attributed to the synergistic effect of CdS and graphene (Wang et al., 2009, 2011).

Kang et al (2009) fabricated CS–GR/GOx modified electrodes for direct electrochemical glucose sensing. The sensor showed excellent performance that was attributed to the large surface area to volume ratio and high conductivity of graphene and the good biocompatibility of chitosan with GOx (Kang et al., 2009).

Dey et al reported a PtNP modified graphene based sensitive ammperometric cholesterol biosensor. The cholesterol oxidase and cholesterol esterase were immobilized on the surface of GR/PtNP for cholesterol detection. The sensitivity and detection limit of the electrode towards cholesterol ester were 2.07 ± 0.1 μA μM^{-1} cm^{-2} and 0.2 μM respectively. The synergistic effect of graphene and PtNP was responsible for high sensitivity and low detection limit (Dey et al., 2010).

Carbon nanomaterials are extensively used for various biological applications including bioimaging and biosensing. Furthermore, the modifications of these carbon nanomaterials are widely used for better applications of imaging probes, biosensors and so on. Also, conjugating various targeting molecules, drugs, genes and contrast agents to carbon nanomaterials is widely investigated in the bioimaging and treatment of cancer cells and tumors. Biological applications of carbon nanomaterials are significantly impacting current biotechnology. Especially, the carbon nanomaterials enable the development of biosensors with enhanced sensitivity, better selectivity and a wide range of detection. Multiple detections have also been achieved with a low LOD and a high sensitivity. The biocompatible properties of carbon nanomaterials make them applicable for in situ detection of living cells.

6. Polymeric Nanomaterial

Conventionally polymers have been considered good electrical insulators. However, Polymers with conjugated π-electron (i. e. system have C=C conjugated bonds) backbones display unusual electronic properties such as low energy optical transition, low ionization potentials, and high

electron affinities. The result is a class of polymers called conducting polymer that can be oxidized or reduced more easily and more reversibly than conventional polymers. The effect of this oxidation or reduction on polymer is called doping, i.e. convert an insulating polymer to conducting one. Conducting Polymers Can provide electromagnetic shielding of electronic circuits, used as antistatic coating material to prevent electrical discharge exposure on photographic emulsions, used as hole injecting electrodes for OLEDS (Kim et al., 2002), used in electroluminescent displays (mobile telephones) and used as emissive layer in full-color video matrix displays.

PEDOT:PSSor **poly(3,4-ethylenedioxythiophene) polystyrene sulfonate** is a polymer mixture of two ionomers. One of the components made up of sodium polystyrene sulfonate which is sulfonated polystyrene. Part of the sulfonyl groups are deprotonated and carry a negative charge. The other component poly(3,4-ethylenedioxythiophene) or **PEDOT** is a conjugated polymer and carries positive charges and is based on polythiophene. Together the charged macromolecules form a macromolecular salt. The combination of an especially low oxidation potential and a relatively low band gap (**~ 1.6 eV**) gives PEDOT some unique electrochemical and spectroscopic properties not accessible in other polymers. As band gap is located at the transition between the visible and near-IR regions of the spectrum, PEDOT is strongly cathodically coloring and transmissive to visible light, sky blue transparent, in the doped and conducting state (oxidized state). The change of the redox state leads to a change in the electronic structure, which is observed as an optical color transition to dark blue. It is for this reason, PEDOT: PSS is called an electro chromic polymer (Jönsson, S. K. M., et al., 2003).

PEDOT:PSS is used as a transparent, conductive polymer with high ductility in different applications. For example, AGFA coats 200 million photographic films per year with a thin, extensively-stretched layer of virtually transparent and colorless PEDOT:PSS as an antistatic agent to prevent electrostatic discharges during production and normal film use, independent of humidity conditions. The unique electrical and optical properties of organic nanostructures such as conducting polymers (CP) [polyaniline (PANI), poly(3,4-ethylenedioxythiophene: poly(4-styrenesulfonate) (PEDOT:PSS) etc] and biopolymers [chitosan (CH), cellulose etc] exhibits the ease in synthesis with desired functionality, solution processability, mechanical flexibility and low cost, which make them promising candidates for a wide range of electronic, optoelectronic

and molecular electronic applications. The charge-transport properties of CP nanomaterials enable sensitive sensing by tuning the CP characteristics. The surface functional groups of CP nanomaterials can be modified covalently using specific bioreceptors, allowing the immobilization of CP nanomaterials on electrode substrates. Therefore, CPs have been predicted to have enough potential for the development of a low cost and high performance biosensor materials that offer high permeability biocompatibility, and rapid electron transfer (Istamboulie, Georges, et al., 2010). However, biomedical applications using CP nanomaterials are still in the early stages. For example, the cellular effects of CP nanomaterials are still not fully characterized, and reliable synthesis routes for CP nanomaterials are still required. A simultaneous-measurement technology for complex single-molecule mixtures should be developed to fabricate human-like artificial bioelectronic noses and tongues. CP nanomaterials have many unexplored potential uses, and we expect future research will lead to the development of many new biomedical applications.

3.6.3. Transducer

A transducer is a device which converts any type of signal to an electrical signal. Thesignal produced as a result of interaction of bio-molecules with the analyte may be in the form ofelectrochemical (change in potential or current), optical (color change), calorimetric (heat measurement), piezoelectric (mass change) response and will be converted to electric signal with the choice of suitable transducer.

3.7. Biosensor for CEA detection

The electrochemical biosensors have recently aroused much interest due to their high signal-to-noise-ratio, simplicity, high sensitivity and fast response time (Kumar et al. 2015; Wang 2006). An electrochemical biosensor is a small device that can be used for direct measurement of the analyte in the sample matrix. Ideally, such a device is capable of responding continuously and reversibly and does not perturb the sample. The development of electrochemical sensors is currently one of the most active areas of analytical research. Electrochemical biosensors hold a

leading position among other classes of sensors and are commercially successful. Electrochemical biosensors combine the analytical prowess of electrochemical techniques and the specificity of biological recognition processes. The most commonly used transducers in electrochemical biosensors are Ammperometric and potentiometric transducers. The analytical information in potentiometric devices is obtained by converting the biological response or biochemical reaction into a potential signal by the use of ionselective electrodes (ISE). Ammperometric biosensors on the other hand monitors the current generated against applied constant potential by the reduction or oxidation of the electroactive species involved in the biorecognition process. Due to high sensitivity and wide linear range, ammperometric biosensors have attracted more attention than its counterpart. The ongoing research on new sensing concepts, combined with numerous technological advancements, has expanded horizons for extensive clinical applications of ammperometric devices (Wang et al., 1999). The enhanced sensitivity, specificity, simplicity, and inherent miniaturization of modern electrochemical bioassays allow them to compete with the most advanced optical protocols (Wang et al., 2006).

Feng et al reported an electrochemical biosensor for label free neoplastic cell detection using aptamer AS1411 and functionalized graphene. The high binding affinity of the aptamer to the overexpressed nucleolin on the neoplastic cell surface enabled the electrochemical aptasensor to detect as low as thousand cells (Feng et al., 2011).

Chen et al developed a simple, label free electrochemical biosensor for oral cancer detection based on nuclease-assisted target recycling and DNAzyme for the detection of DNA species related to oral cancer in saliva (Chen et al., 2011).

S.No.	Nanostructured matrix	Fabrication Method	Biomarker used	Detection technique	Sensing parameter	References
1.	PEDOT:PSS/RGO	Dip coating	CEA	Amperometry	[L]= 2-8 $ngmL^{-1}$ [S]= 25.8 $\mu Ang^{-1}mL$	Kumar et al BSB 2014
2.	PEDOT:PSS/CNT	Dip coating	CEA	Amperometry	[L]= 2-15 $ngmL^{-1}$ [S]= 7.8 $\mu A\ ng^{-1}mL$	Kumar et al BSB 2014
4.	Carbon paste, wax, MWCNT, chitosan and HRP	Wax printing, Screen printing	α-fetoprotein (AFP), carcinoma antigen 125 (CA125), carcinoma antigen 199 (CA199) carcinoembryonic antigen (CEA)),	Differential pulse voltametery (DPV)	AFP: [L]= 0.05-95$ngmL^{-1}$ [LOD]= 0.01 $ngmL^{-1}$ CA125: [L]= 0.02-85UmL^{-1} [LOD]= 6 $mUmL^{-1}$ CA199: [L]= 0.005-120 UmL^{-1} [LOD]= 8$mUmL^{-1}$ CEA: [L]= 0.05-105$ngmL^{-1}$ [LOD]= 5 $pgmL^{-1}$ [T]= 4 Weeks	Zang et al ChemComm 2012
5.	Gold NPs on SPE	Wax Printing Screen Printing	CEA	Cyclic Voltammetry	[L]= 0.001-1.0 $ngmL^{-1}$ [LOD]= 0.85 $pgmL^{-1}$ [S]= 4 weeks	Wang et al RSC 2014
6.	Graphene oxide/ chitosan on SPE,	Screen Printing	Carcino embryonic	Differential Pulse Voltammetry	CEA and AFP [L]= 0.01–100 $ngmL^{-1}$	Wu et al Anal. Chem.

	Carbon ink, Ag/AgCl ink		Antigen (CEA) Alpha fetoprotein (AFP) Cancer Antigen 125 (CA125) Carbohydrate Antigen 153 (CA153)		[LOD]= 0.01 ng mL^{-1} [T]= 3 weeks CA125 and CA153 [L]= 0.05–100 ng mL^{-1} [LOD]= 0.05 ng mL^{-1} [T]= 3 weeks	2013
7.	Multi-walled Carbon nanotubes (MWCNTs), Carbon ink, Ag/AgCl ink Screen Printed Electrode	Wax Printing, Screen Printing	CEA CA125	Differential Pulse Voltammetry	CEA [L]= 0.05–50 ng mL^{-1} [LOD]= 0.01 ng mL^{-1} [T]=4 weeks CA125 [L]= 0.001–75 U mL^{-1} [LOD]= 0.2 mU mL^{-1} [T]= 4 weeks	Wang et al Biosensors and Bioelectronics 2011
8.	Polyaniline(PANI) on SPE, Graphite and silver paste	Screen Printing	Interleukin-2 receptor alpha	Cyclic Voltammetry	[L]= 0.5–3 ng ml^{-1} [S]= 0.737 mA ng^{-1} mL^{-1} cm^{-2}	Kumar et al RSC 2013
9.	Graphene oxide-Chitosan, Gold NPs on SPE	Wax Printing Screen Printing	Prostate Protein Antigen (PPA) Carcino embryonic Antigen (CEA)	Electrochemical Impedance Spectroscopy [EIS]	PSA [L]= 0.003–20 ngmL^{-1} [LOD]= 1 pgmL^{-1} [T]= 4 weeks CEA [L]= 0.001–10ngmL^{-1} [LOD]= 0.8 pgmL^{-1} [T]= 4 weeks	W. Li et al. 2013 AnalyticaChimicaActa

10.	CNTs/Chitosan/ Glutaraldehyde on SPE Carbon Nanodots	Wax Printing Screen-printing	Carcino embryonic antigen (CEA) Alpha-fetoprotein (AFP) Cancer antigen 199 (CA199) Carcinoma antigen 153 (CA153)	Electrochemical Impedance Spectroscopy [EIS]	CEA [L]= 4.0 pgmL^{-1} AFP [L]= 0.02 ngmL^{-1} CA199 [L]= 6.0mUmL^{-1} CA153 [L]= 5.0 mUmL^{-1}	Wang et al., 2012 Lab Chip, RSC
11.	ZnO nanorods LED/ CPWE/CNT / CDs	CPWE Wax Printing/ Screen Printing ZnO NR Pulsed Layer Deposition	Carcino embryonic Antigen (CEA) Cancer Antigen 125 (CA125) Cancer Antigen 15-3 (CA15-3)	Electro-luminescence	CEA [L]= 0.005-20 ng mL^{-1} [LOD]= 1.8 pg mL^{-1} CA 125 [L]= 0.01–50 ng mL^{-1} [LOD]= 3.6 pg mL^{-1} CA 15-3 [L]= 0.01-50 ng mL^{-1} [LOD]= 3.8 pg mL^{-1}	Zhang et al Chem. Comm 2014

S.No.	Nanostructured matrix	Fabrication Method	Biomarker used	Detection technique	Sensing parameter	References
3.	PEDOT:PSS/RGO	Dip coating	CEA	Amperometry	[L]= 2-8 ngmL^{-1} [S]= 25.8 µAng^{-1}mL	Kumar et al BSB 2014

4.	PEDOT:PSS/CNT	Dip coating	CEA	Amperometry	[L]= 2-15 $ngmL^{-1}$ [S]= 7.8 µA $ng^{-1}mL$	Kumar et al BSB 2014
4.	Carbon paste, wax, MWCNT, chitosan and HRP	Wax printing, Screen printing	α-fetoprotein (AFP), carcinoma antigen 125 (CA125), carcinoma antigen 199 (CA199) carcinoembryonic antigen (CEA)),	Differential pulse voltametery (DPV)	AFP: [L]= 0.05-95$ngmL^{-1}$ [LOD]= 0.01 $ngmL^{-1}$ CA125: [L]= 0.02-85UmL^{-1} [LOD]= 6 $mUmL^{-1}$ CA199: [L]= 0.005-120 UmL^{-1} [LOD]= 8$mUmL^{-1}$ CEA: [L]= 0.05-105$ngmL^{-1}$ [LOD]= 5 $pgmL^{-1}$ [T]= 4 Weeks	Zang et al ChemComm 2012
5.	Gold NPs on SPE	Wax Printing Screen Printing	CEA	Cyclic Voltammetry	[L]= 0.001-1.0 $ngmL^{-1}$ [LOD]= 0.85 $pgmL^{-1}$ [S]= 4 weeks	Wang et al RSC 2014
6.	Graphene oxide/ chitosan on SPE, Carbon ink, Ag/AgCl ink	Screen Printing	Carcino embryonic Antigen (CEA) Alpha fetoprotein (AFP) Cancer Antigen	Differential Pulse Voltammetry	CEA and AFP [L]= 0.01–100 $ngmL^{-1}$ [LOD]= 0.01 ng mL^{-1} [T]= 3 weeks CA125 and CA153	Wu et al Anal. Chem. 2013

			125 (CA125) Carbohydrate Antigen 153 (CA153)		[L]= 0.05–100 ng mL^{-1} [LOD]= 0.05 ng mL^{-1} [T]= 3 weeks	
7.	Multi-walled Carbon nanotubes (MWCNTs), Carbon ink, Ag/AgCl ink Screen Printed Electrode	Wax Printing, Screen Printing	CEA CA125	Differential Pulse Voltammetry	CEA [L]= 0.05–50 ng mL^{-1} [LOD]= 0.01 ng mL^{-1} [T]=4 weeks CA125 [L]= 0.001–75 U mL^{-1} [LOD]= 0.2 mU mL^{-1} [T]= 4 weeks	Wang et al Biosensors and Bioelectronics 2011
8.	Polyaniline(PANI) on SPE, Graphite and silver paste	Screen Printing	Interleukin-2 receptor alpha	Cyclic Voltammetry	[L]= 0.5–3 ng ml^{-1} [S]= 0.737 mA ng^{-1} mL^{-1} cm^{-2}	Kumar et al RSC 2013
9.	Graphene oxide-Chitosan, Gold NPs on SPE	Wax Printing Screen Printing	Prostate Protein Antigen (PPA) Carcino embryonic Antigen (CEA)	Electrochemical Impedance Spectroscopy [EIS]	PSA [L]= 0.003–20 ngmL^{-1} [LOD]= 1 pgmL^{-1} [T]= 4 weeks CEA [L]= 0.001–10ngmL^{-1} [LOD]= 0.8 pgmL^{-1} [T]= 4 weeks	W. Li et al. 2013 AnalyticaChimicaActa
10.	CNTs/Chitosan / Glutaraldehyde on SPE	Wax Printing Screen-printing	Carcino embryonic antigen (CEA)	Electrochemical Impedance Spectroscopy [EIS]	CEA [L]= 4.0 pgmL^{-1} AFP	Wang et al., 2012 Lab Chip, RSC

	Carbon Nanodots		Alpha-fetoprotein (AFP) Cancer antigen 199 (CA199) Carcinoma antigen 153 (CA153)		CA199 [L]= 6.0mUmL^{-1} CA153 [L]= 5.0 mUmL^{-1}	
11.	ZnO nanorods LED/ CPWE/CNT / CDs	CPWE Wax Printing/ Screen Printing ZnO NR Pulsed Layer Deposition	Carcino embryonic Antigen (CEA) Cancer Antigen 125 (CA125) Cancer Antigen 15-3 (CA15-3)	Electro-luminescence	CEA [L]= 0.005-20 ng mL^{-1} [LOD]= 1.8 pg mL^{-1} CA 125 [L]= 0.01–50 ng mL^{-1} [LOD]= 3.6 pg mL^{-1} CA 15-3 [L]= 0.01-50 ng mL^{-1} [LOD]= 3.8 pg mL^{-1}	Zhang et al Chem. Comm 2014

[L]- Linear range, [LOD]- Limit of Detection, [S]- Sensitivity, [T]- Time period (stability)

Table 2: - Nanomaterials integrated biosensor for CEA detection

Chapter-4

Materials and Methods

4.1. Chemical and reagents

PEDOT:PSS (1.3 wt%, PEDOT content: 0.5wt%, PSS content: 0.8 wt%),Graphite powder flakes (45 µm, >99.99 wt%) carcinoembryonic antibody monoclonal (anti-CEA), carcinoembryonic antigen (CEA), 1-(3-(dimethylamino)-propyl)-3-ethylcarbodiimide hydrochloride (EDC) ($C_8H_{17}N_3$) and bovine serum albumin (BSA) of AR grade were procured from Sigma Aldrich, India. Sodium hydroxide (NaOH) pellets, sodium monophosphte (NaH_2PO_4), sodium diphosphatedihydrate ($Na_2HPO_4.2H_2O$), N-hydroxysulfosuccinimide (NHS) ($C_4H_5NO_3$) sodium chloride (NaCl), acetonitrile (ACN), potassium ferricyanide $\{K_3[Fe(CN)_6]\}$ and potassium ferrocyanide $\{K_4[Fe(CN)_6]3H_2O\}$ were purchased from Fisher Scientific. All the chemicals were of analytical grade and were used without any further purification. Phosphate buffer saline (PBS) solution of pH 7.0 was prepared using $Na_2HPO_4.2H_2O$ (0.05 mol L^{-1}) and NaH2PO4 (0.05 mol L^{-1}). Fresh PBS solution was prepared using Milli-Q water having resistivity of 18 MO cm and stored at 4 °C. The monoclonal antibody and CEA antigen biomolecules were further diluted using PBS buffer of pH 7.0.

4.2. Experimental

4.2.1 Preparation of graphene oxide (GO) suspension

Graphite powder (<20 µm) obtained from Sigma Aldrich was used to synthesize Graphite oxide by the modified Hummers method which was further exfoliated to obtain a brown colored graphene oxide (GO) dispersion under ultrasonication. In the aforementioned method, a mixture of graphite powder (1.0 g), P_2O_5 (0.50 g) and $K_2S_2O_8$ (0.50 g) was added to 3.0 mL of conc. H_2SO_4 and stirred continuously until the reactants are completely dissolved in the acid. Then the obtained mixture in placed in a hot air oven at 80°C for 4.5 hours post which the mixture is removed and diluted with 1.0 L Millipore water. The diluted mixture is then filtered and further washed to remove all traces of the acid. The pretreated graphite is then added to 26 mL of H_2SO_4 and stirred for the oxidation step of the synthesis. 3.0 g of $KMnO_4$ was added to the reaction mixture in an ice bath so that the temperature does not exceed 10°C. The temperature of the reaction mixture was increased to 35°C and maintained for 2 hours post which the heat was removed and 46 mL of distilled water is added under an ice bath. Again the temperature of the

reaction mixture was increased to 35°C and was continuously stirred for 2 hours, post which the heat was removed and the mixture was diluted with 140 mL of water and 2.5 mL of 30% H_2O_2 which imparts yellow color to the mixture along with bubbling. The mixture is then left undisturbed for a day allowing it to settle and later the supernatant is decanted. The remaining mixture is the filtered and washed with a 1.0 L of 10% HCl solution. The obtained solid is air dried and diluted in distilled water which is put through two weeks of dialysis to remove any remaining residues or impurities. The dialyzed product is further centrifuged and washed several times with Millipore water to neutralize and remove residues. Finally, the product was dried in a vaccum oven at 50°C for a day resulting in dark brown GO powder. To obtain a stable suspension of GO (conc. 0.50 mg/mL), the obtained GO powder was dissolved in a known volume of water and ultrasonicated for 40 minutes. This was further centrifuged at 4000 rpm for 10 min to remove any aggregates remained in the suspension.

4.2.2 Preparation of Reduced Graphene Oxide (RGO) with Hydrazine in the presence of PEDOT:PSS

The stable GO suspension (20.0 mL, 0.50 mg/mL) obtained by modified hummers method was mixed with 7.70 mL of PEDOT:PSS (Sigma Aldrich) solution (1:10 w/w ratio vs. GO, total 1.3 wt % dispersion in water, 0.50 wt% of PEDOT, and 0.80 wt% of PSS). A stable suspension of RGO nanosheets functionalized with PEDOT:PSS (RGO/PEDOT) was obtained upon addition of 60.0 μL of hydrazine solution (35 wt% in water, Aldrich) to the suspension, and heating the reaction mixture at 95°C for 3 hours. After the reaction, the suspension was filtered with polyvinylidene fluoride (PVDF) membrane filter (pore size of 0.45 μm) through a vaccum filter setup. The obtained filtrate was washed thoroughly with Millipore water to remove any residual hydrazine and unbound PEDOT:PSS polymer, yielding a thin film of RGO/PEDOT nanocomposite. The nanocomposite was dried under ambient conditions and the obtained hybrid film was crushed and stored for later use.

4.2.3 Electrophoretic fabrication of PEDOT/RGO/ITO electrode

PEDOT/RGO films are fabricated onto an ITO coated glass substrate via the electrophoretic deposition (EPD) technique. 10 mL colloidal solution of PEDOT/RGO (1.0 mg mL^{-1}, 10 mg PEDOT/RGO nanocomposite powder dissolved in 10 mL acetonitrile) is used for EPD. The electrophoretic deposition was carried out using a two-electrode cell containing the colloidal suspension by applying DC voltage (50 V) for 2 min. In order to obtain a surface charge on the RGO,10^{-5} to 10^{-4}mol of Mg $(NO3)_2$.6H2O is added into the suspension as an electrolyte for EPD. Mg^{2+} ions adsorbed by the RGO sheets provide an adequate positive surface charge to the RGO sheets apart from the positive charge of the PEDOT particles, resulting in enhanced deposition rate at the anode (ITO). Platinum (Pt) foil (1 cm x 2 cm)acts as the cathode and a pre-cleaned ITO-coated glass substrate(sheet resistance of 30 Ω cm^{-1}) as the anode. The two electrodes separated by 1 cm are placed parallel to each other, dipped in the PEDOT/RGO colloidal suspension. The deposited film is removed from the suspensions and is washed with deionized water followed by drying.

4.2.4 Fabrication of BSA/anti-CEA/PEDOT/RGO/ITO immunoelectrode

Monoclonal anti-carcinoembryonic (anti-CEA) antibody, carcinoembryonic (CEA) antigen, N-ethyl-N-(3-dimethylaminopropyl) carbodiimide (EDC),N-hydroxysuccinimide (NHS) and bovine serum albumin (BSA)have been procured from Sigma-Aldrich.

For the fabrication of bioelectrode monoclonal CEA (1 mg/mL) were immobilized onto the PEDOT/RGO/ITO electrode via covalent bonding using the EDC-NHS chemistry. Monoclonal anti-CEA antibody solution is freshly prepared in phosphate buffer (PBS, pH 7.4).Prior to the covalent immobilization process, a cocktail of EDC, NHS and anti-CEA antibodies is made in the ratio 1:1:2.Then 30 µL of this cocktail is applied on the PEDOT/RGO/ITO electrode as a result of which the COO group of the RGO/ITO electrode is activated by EDC as the coupling agent and NHS as activator. Post the immobilization process the anti-CEA/PEDOT/RGO/ITO electrode is incubated in a humid chamber for about 4 hours at room temperature. The covalent interaction is proposed to occur via the formation of a strong amide (CO–NH) bond between the carboxyl group of RGO and the amino terminal of the anti-CEA. Bovine serum albumin (BSA)

solution (1 $mgmL^{-1}$) is used to block the non-specific active sites of the electrode. The BSA-anti-CEA/PEDOT/RGO/ITO immunoelectrode is then washed with PBS and stored at 4 ˚C, when not in use.

4.3 Characterization

Crystallinity and phase information of synthesized product was obtained by using monochromatic X-ray diffraction (XRD) pattern [Bruker D-8 Advance] with Cu-Ka radiation (**λ**=1.5406 Å). Morphological observations and particle size were carried out using transmission electron microscopy at an accelerating voltage of 200 kV (Tecnai G2 30 U-twin, Tecnai 300 kV ultrathin microscope) and scanning electron microscopy (Nova Nano Sem450 and Carl Zeiss, EVO15). The Autolab Potentiostat(Netherlands) was used for the electrochemical response studies by using a three-electrode system. The fabricated electrode acted as the working electrode, Ag/AgCl as the reference electrode and platinum (Pt) as the counter electrode.

4.3.1 X-ray diffraction (XRD) technique

Max von Laue, in 1912, discovered that crystalline substances act as three- dimensional diffraction gratings for X-ray wavelengths similar to the spacing of planes in a crystal lattice. X-ray diffraction is an effective tool in studying the nature of crystalline substances. It is based on constructive interference of monochromatic X-rays and a crystalline sample. These X-rays are generated by a cathode ray tube, filtered to produce monochromatic radiation, collimated to concentrate, and directed toward the sample. The interaction of the incident rays with the sample produces constructive interference (and a diffracted ray) when conditions satisfy Bragg's Law (**Eq. 1**)

$$2d \, Sin\, \theta = n\, \lambda \ldots\ldots\ldots\ldots \text{ Eq. 1}$$

Where λ is the wavelength of electromagnetic radiation, θ is the diffraction angle and d is the lattice spacing in a crystalline sample. These diffracted X-rays are then detected, processed and counted. By scanning the sample through a range of 2θ angles, all possible diffraction directions

of the lattice is attained due to the random orientation of the powdered material. This technique is used to characterize the crystallographic structure, crystallite size (grain size) and preferred orientation in polycrystalline or powder solid samples.

XRD can be applied to characterize the heterogeneous solid mixture to determine relative abundance of a crystalline compound. It is also useful in providing information on the structure of unknown sample when coupled with lattice refinement technique such as relative refinement. XRD patterns are recorded on X-ray diffractometer, wherein the peak broadening data are obtained by measuring the average of peak broadening in the five strongest diffraction peaks. The mean size of the nanoparticles is determined from the peak broadening in the X-ray diffraction pattern by using Debye– Scherrer equation (Eq. 2).

$$\mathbf{D} = \frac{\mathbf{0.9}\,\boldsymbol{\lambda}}{\boldsymbol{\beta Cos\theta}} \quad \text{..... Eq. 2}$$

Where D is the average crystallite size (Å), λ is wavelength of X-rays (Cu Kα: λ = 1.5418 Å), θ is the Bragg diffraction angle, and β is the full width at half maximum (FWHM) (in radians). The sample under study can be of either a thin layer of crystal or in powder form. Since the power of a diffracted beam is dependent on quantity of corresponding crystalline substance; it is also possible to carry out quantitative determinations using this technique.

4.3.2 Transmission Electron Microscopy (TEM)

It is a microscopic technique in which a beam of electron passes through an ultra-thin specimen for the interaction with sample. Electrons are accelerated with 100 KeV-1 MeV to project onto a specimen of less than 200 nm through the help of condenser lens system. The interaction of electron beam and sample results in image formation which is further focused and magnified on imaging device or detected by the CCD camera. TEM provides high-resolution images (ranging from 50 to 10^6) than the light microscope.

A TEM is constituted of: (1) two or three condenser lenses to focus the electron beam on the sample, (2) an objective lens to form the diffraction in the back focal plane and the image of the sample in the image plane, (3) some intermediate lenses to magnify the image or the diffraction pattern on the screen. TEM is commonly operated in Bright Field (BF) imaging mode. In BF

mode the contrast formed directly by absorption and occlusion of electrons in the sample. Sample regions with thickness or higher atomic number will appear dark and the region with no sample will appear bright. Other then structural characterization of nanomaterials (NMs) TEM can also be used to determine NM's melting point. The melting point of NMs determine by the electron diffraction disappearance which results due to the heat up of NMs with electron beam. Beside this TEM also can be used to study the electrical and mechanical properties of nanotubes and nanowires.

4.3.3 Scanning Electron Microscope (SEM)

It is a microscopic technique that uses a focused beam of high-energy electrons to generate a variety of signals at the surface of solid specimens. The signals that derive from electron-sample interactions reveal information about the sample including external morphology (texture), chemical composition, and crystalline structure and orientation of materials making up the sample. In most applications, data are collected over a selected area of the surface of the sample, and a 2-dimensional image is generated that displays spatial variations in these properties. Areas ranging from approximately 1 cm to 5 microns in width can be imaged in a scanning mode using conventional SEM techniques (magnification ranging from 20X to approximately 30,000X, spatial resolution of 50 to 100 nm).

4.3.4 Electrochemical Techniques

Electrochemical techniques relate the changes of an electrical signal to an electrochemical reaction at an electrode surface, usually as a result of an imposed potential or current. In a solution, the equilibrium concentrations of the reduced and oxidized forms of a redox couple are linked to the potential (E) via the **Nernst's Equation (Eq. 3)**.

$$E = E_o + \frac{RT}{nF} \ln \frac{Coxi}{Cred} \quad \text{..... Eq. 3}$$

where, E_o is equilibrium potential, F is Faraday's constant, T is absolute temperature, C_{oxi} and C_{red} are concentrations of oxidation and reduction centers. If the potential E is applied to the

working electrode with respect to the reference electrode e.g. via Potentiostat, thereof couples present at the electrode respond to this change and adjust their concentration ratios according to Eq. 3.

Cyclic voltammetry is a versatile potentiodynamic electroanalytical technique that is employed to study t h e electrochemical properties of electroactive species. To obtain a cyclic voltammogram, the voltage is varied in the solution and change in current is measured with respect to the change in voltage. It is an electrolytic method that uses microelectrodes and an unstirred solution so that the measured current is limited by analyte diffusion at an electrode surface.

In a CV experiment, current response over a range of potentials (a potential window) is measured, starting at an initial value and varying the potential in a linear manner up to a pre-defined limiting value. The current increases as the voltage reaches the oxidation potential of the analyte, after which it falls off as the concentration of the analyte is depleted close to the electrode surface. At this potential (often referred to as a switching potential), the direction of the potential scan is reversed, and the same potential window is scanned in the opposite direction (hence the term cyclic). As the applied potential is reversed, it will reach a potential where the reduction of product formed during forward scan starts producing a current of reverse polarity from the forward scan. This reduction peak will usually have a similar shape as that of an oxidation peak in other direction. Non-symmetric peaks are attributed to a quasi-reversible reaction. If the process is completely irreversible, the anodic peak does not appear in the measurable potential region. As a result, information about the redox potential and nature of electrochemical reactions is obtained. The important parameters that can be derived from CV are magnitude of peak current (*Ip*), peak potential (*Ep*), number of electrons transferred per reactant molecule (*n*), rate constant, diffusion coefficient (*D*) and electrochemical reversibility. The peak Current (*Ip*) for a reversible system is described by the **Randles-Sevcik equation (Eq. 4)**

$$\mathbf{I_p = (2.69 \times 10^5)\, n^{3/2} A D^{1/2} C v^{1/2}} \quad \text{…… Eq. 4}$$

Differential pulse voltammetry (DPV) is one of the most commonly used pulse techniques in electrochemistry. Electrochemical pulse methods involve the modulation of potential in order to increase speed and sensitivity of measurement. DPV consists of a series of potential pulses of fixed amplitude (10-100 mV) superimposed on to a slowly changing base potential. The time

interval of each potential step in this series is ~40-50 smother current is measured at two time points of the pulse – first, just before the pulse starts and second when the pulse ends. The difference between the current values at these two points (δi) is plotted against the base potential. The resulting plot of δi vs. V is referred to as a differential pulse voltammogram consisting of current peak(s), the height of which is directly proportional to the concentration of the corresponding analyte(s). The relationship between the peak current and concentration of analyte is given by the following equation **(Eq. 5)**

$$\mathbf{I_p} = \frac{\boldsymbol{nFAD^{1/2}C}}{\sqrt{\boldsymbol{\pi t_m}}} \frac{\boldsymbol{(1-\sigma)}}{\boldsymbol{(1+\sigma)}} \text{ …….. Eq. 5}$$

where n is the no. of electrons involved, F is Faraday's constant, A is electroactive surface area, D is diffusion coefficient, C is the concentration of the electroactive species, t_m is the time after pulse when current is sampled, and $\sigma = \exp[(nF/RT)(\Delta E/2)]$ (ΔE is the pulse amplitude). For large values of ΔE, the maximum value of $(1-\sigma)/(1+\sigma)$ is unity.

Chapter-5

Results and Discussion

5.1 Structural and morphological studies

The Crystallinity and phase information of synthesized nanocomposite was obtained by using monochromatic X-ray diffraction (XRD) pattern [Bruker D-8 Advance] with Cu-Ka radiation (**λ**=1.5406 Å).The X-ray diffraction (XRD) pattern of powder nanocomposite of PEDOT/RGO in the range 10-50˚ is shown in the **figure 2**. A broad peak at 2θ= 24.15˚ corresponding to (002) reflection plane confirms the presence of reduced graphene oxide (RGO) in the nanocomposite (**Srivastava et al., 2013**). Another broad peak at 2θ= 25.68˚ confirms the presence of Poly (3,4-ethylene dioxythiophene) (PEDOT) in the nanocomposite (**K. Singh et al., 2007, Kokate et al., 2015**). The broadened peaks in the pattern indicate formation and presence of PEDOT/RGO nanocomposite

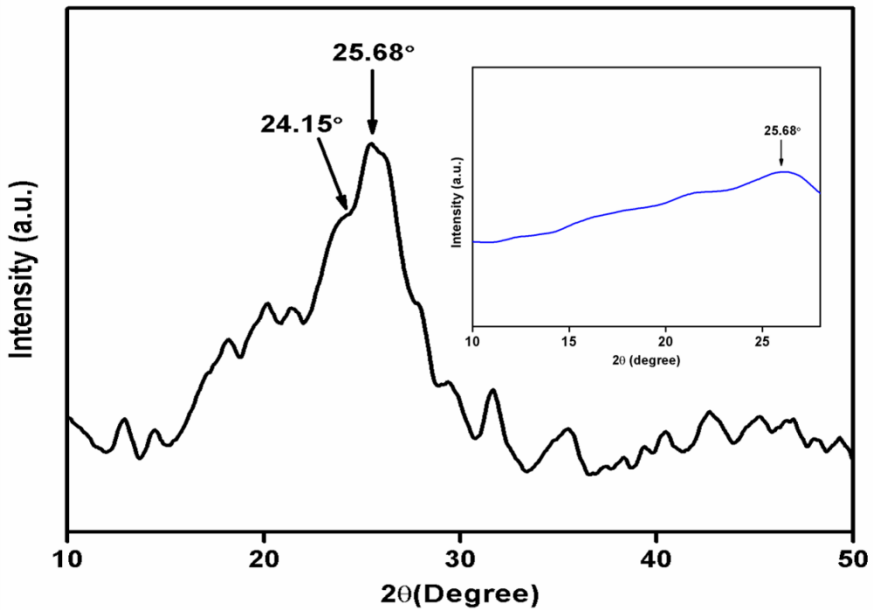

Figure 2. XRD pattern showing peaks for RGO (24.15˚) and PEDOT (25.68˚)

The morphology of the synthesized PEDOT/RGO nanocomposite was investigated by transmission electron microscopy (TEM) and scanning electron microscopy (SEM) images. For the TEM studies a well dispersed solution of PEDOT/RGO nanocomposite was prepared in milli-Q water and dropped onto 50 mesh carbon coated copper grid. This is dried at room temperature and then utilized for TEM studies. The TEM images reveal the shape and size of the PEDOT nanoparticles. **Figure 3a** shows agglomeration of PEDOT particles and that these

PEDOT particles are spherical in shape and uniformly grafted onto the RGO sheet. **Figure 3b** clearly indicates reduced graphene oxide sheets and some are overlapped. The brighter area in the TEM image is attributed to thin layered RGO (red dotted line) and the darker region corresponds to PEDOT particles (yellow dotted line). The TEM image was used to determine the size of PEDOT nanoparticles which was found to have an average diameter of 20 nm. **Figure 3 (c-d)** shows SEM images of the PEDOT/RGO nanocomposite and antibody immobilized and BSA blocked nanocomposite film. **Figure 3c** clearly shows uniform spherical PEDOT nanoparticles with layered RGO sheets. The inset of **figure 3c** is a magnified image of the PEDOT nanoparticles further confirming their spherical shape as indicated by TEM. **Figure 3d** shows the uniformly immobilized anti-CEA antibodies on the nanocomposite which was further blocked with BSA to block any non specific sites.

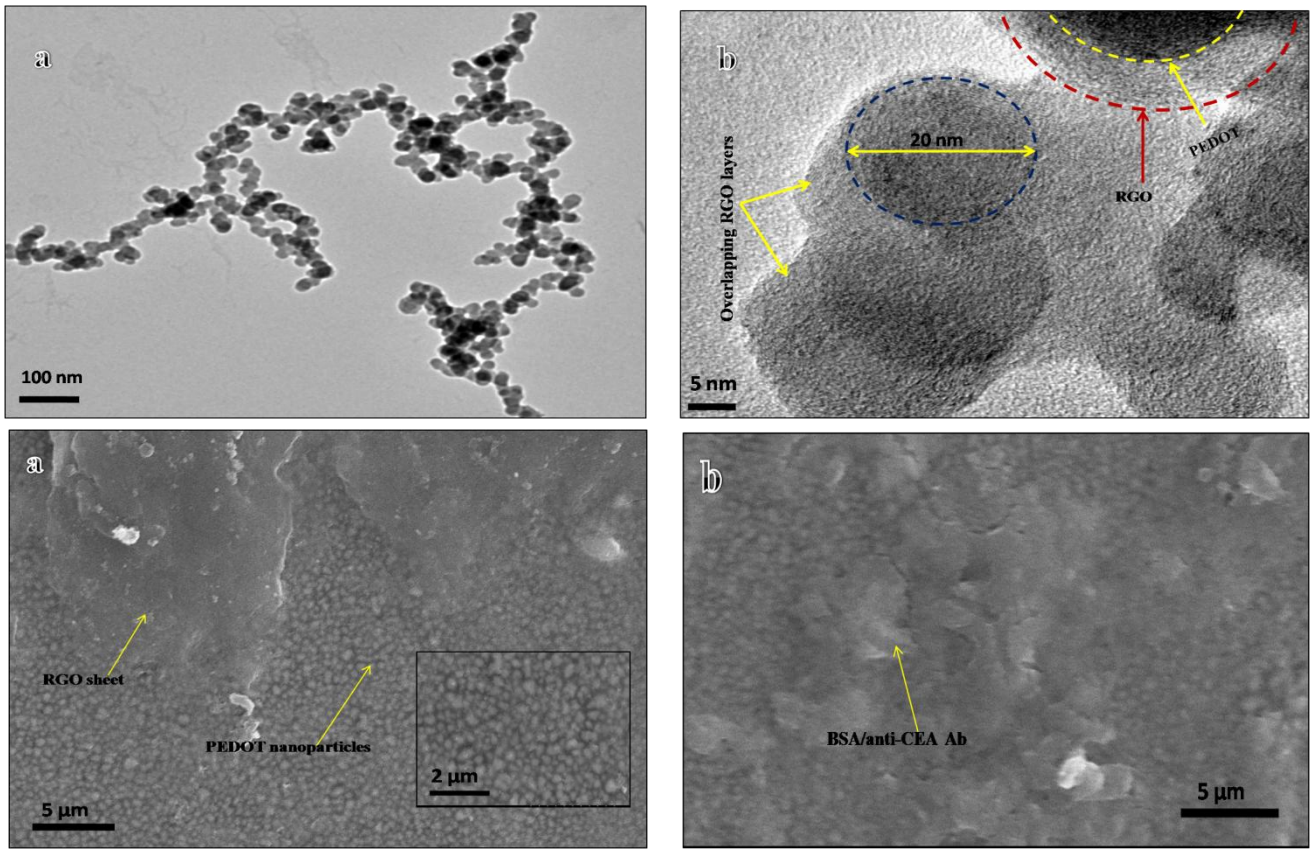

Figure 3. (a-b) TEM images and (c-d) SEM images. Inset of figure 3c is magnified PEDOT nanoparticles

5.2 Electrochemical Studies

The pH studies have been conducted on the fabricated immunoelectrode (BSA/anti-CEA/PEDOT/RGO/ITO) using cyclic voltammetry (CV) in PBS (50 mM, 0.9% NaCl) buffer at different pH 6.0, 6.5, 7.0, 7.4, 8.0, with $[Fe(CN)6]^{3-/4-}$ (5mM) at scan rate of 50 mV/s in the potential range -0.8 to 0.8 V. It has been found that this electrode exhibits maximum current at pH 7.0 (**Figure 4**). This may be due to the fact that biological molecules (such as amino acid, enzyme, antigen, antibody etc.) are present in natural form with high activity at neutral pH. However, in acidic or basic medium antibodies get denatured due to the effect of H^+ or OH^- ions on the amino acid sequence of antibody.(Kumar et al. 2011; Liu and Lin 2005) Therefore, further electrochemical measurements have been performed in the buffer with pH 7.0.

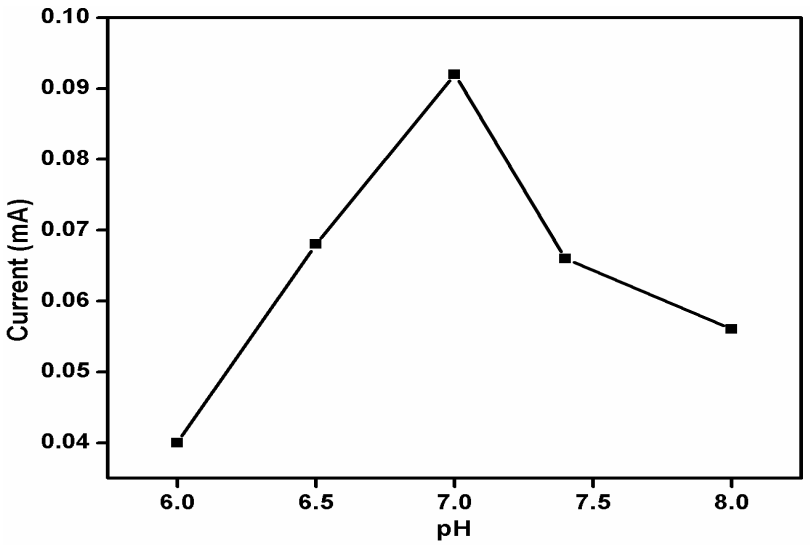

Figure 4.pH response of BSA/anti-CEA/PEDOT/RGO/ITO

The differential pulse voltammetry(DPV) of ITO, PEDOT/RGO/ITO, anti-CEA/PEDOT/RGO/ITO, and BSA/anti-CEA/PEDOT/RGO/ITO electrodes have been recorded (**Figure 5**). The magnitude of current obtained for bare ITO electrode (I_{pa}= 0.310 mA) is significantly higher than that obtained for PEDOT/RGO/ITO electrode (I_{pa}= 0.140 mA) indicating decreased electron transfer between solution and PEDOT/RGO/ITO interface. Though

an increase in the magnitude of the current (I_{pa}= 0.215 mA) with peak potential shifting to a lower value was observed on immobilization of anti-CEA antibodies onto the PEDOT/RGO/ITO electrode indicating facile electron transfer to the electrode surface. The magnitude of current response increases after anti-CEA functionalizes the PEDOT/RGO/ITO electrode surface. One reason for increase in the magnitude of current is the presence of nanocomposite PEDOT/RGO, a mediator on electrode surface that considerably shortens the electron tunneling distance between the antibodies and the electrode. The nanocomposite provides favorable microenvironment and spatial orientation for antibodies molecules resulting in higher magnitude of current (**Suveen et al., 2015**). Apart from this, the electrostatic interaction between the free site of the antibodies (-NH 2 terminal) and the redox species may result in fast electron diffusion toward the immunoelectrode decrease in the magnitude of current to I_{pa}= 0.164 mA was observed upon immobilization of Bovine serum albumin (BSA) as a result of nonspecific adsorption of BSA onto the exposed PEDOT/RGO sites of the anti-CEA/PEDOT/RGO/ITO immunoelectrode that hinders electron transfer between solution and immunoelectrode. After the BSA treatment, the peak potential shifts toward the higher value due to insulating characteristics of the BSA molecules.

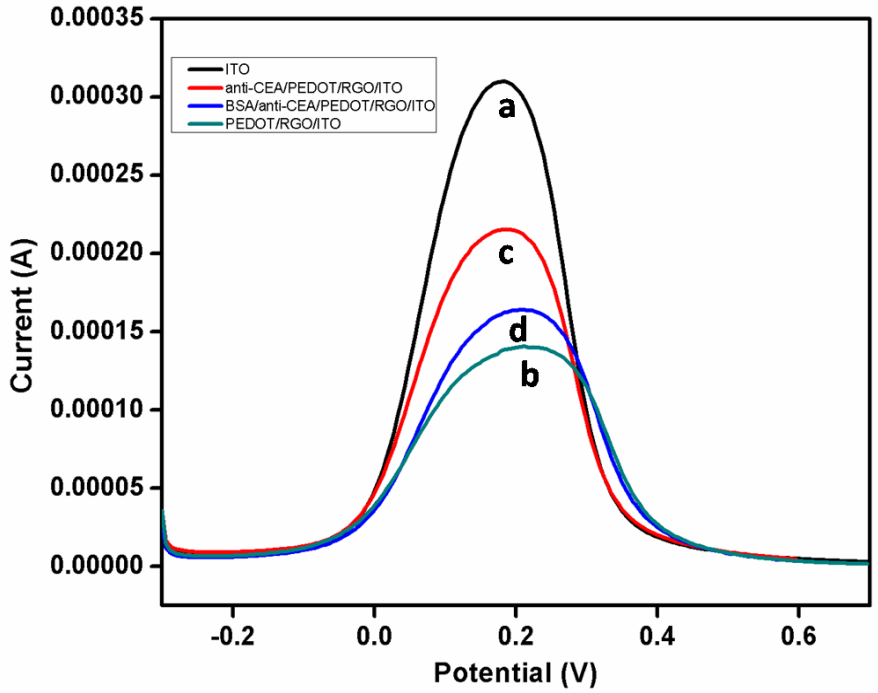

Figure 5.Differential pulse voltammetry (DPV) electrode response study of (a) ITO electrode, (b) PEDOT/RGO/ITO, (c) anti-CEA/PEDOT/RGO/IT and (d) BSA/anti-CEA/PEDOT/RGO/ITO

Scan rate response studies recorded between 40-160 mV/s of fabricated PEDOT/RGO/ITO electrode and BSA/anti-CEA/PEDOT/RGO/ITO immunoelectrode as shown in the **figure 6** and **figure 7**respectively show a linear electrochemical anodic (I_{pa}) and cathodic (I_{pc}) peak current (as shown in figure 6 and 7, **inset a**) that follows equations (i) to (iv). Linear electrochemical response indicated that the electrochemical reaction is a diffusion controlled process.

I_{pa} (PEDOT/RGO/ITO)= {123.21µA(s/mV) x (scan rate[mV/s])$^{1/2}$} + 193µA, R^2= 0.999 …(i)

I_{pc} (PEDOT/RGO/ITO) = -{120.97 µA(s/mV) x (scan rate [mV/s])$^{1/2}$} – 164 µA, R^2= 0.998 ...(ii)

I_{pa} (BSA/anti-CEA/PEDOT/RGO/ITO)={67.89 µA (s/mV) x (scan rate [mV/s])$^{1/2}$} + 130 µA, R^2 = 0.997 …(iii)

I_{pc} (BSA/anti-CEA/PEDOT/RGO/ITO)= -{63.37 µA (s/mV) x (scan rate [mV/s])$^{1/2}$} – 138 µA, R^2= 0.998 …(iv)

Electrochemical response study of PEDOT/RGO/ITO electrode and BSA/anti-CEA/PEDOT/RGO immunoelectrode demonstrated a linear relationship (linear regression coefficient R^2= 0.999 between potential peak shifts ($\Delta V = V_{pa} - V_{pc}$) and square root of scan rate (as shown in the figure 6 and 7, **inset b**) where V_{pa} is anodic peak potential and V_{pc} is cathodic peak potential. Linearity graphs follow the equations (v) and (vi).

ΔV (PEDOT/RGO/ITO)= {0.029 V (s/mV) x (scan rate [mV/s])$^{1/2}$} + 0.09 V, R^2= 0.999 …(v)

ΔV(BSA/anti-CEA/PEDOT/RGO/ITO)= {0.030 V (s/mV) x (scan rate [mV/s])$^{1/2}$} + 0.10 V, R^2= 0.999 … (vi)

This linear relationship indicates that the fabricated immunoelectrode is highly stable as well as an efficient electron transfer platform that can be used as a sensing platform for detecting cancer biomarker Carcinoembryonic Antigen (CEA). Diffusion coefficient (D) of the redox species from the medium to the BSA/anti-CEA/PEDOT/RGO/ITO immunoelectrode is calculated using **Randles-Sevcik** equation.

$$I_p = (2.69 \times 10^5)\, n^{3/2} A D^{1/2} C v^{1/2} \quad \ldots\ldots\ldots\ldots\ldots \text{(vii)}$$

Where,

'I_p' is the peak current of the BSA/anti-CEA/PEDOT/RGO/ITO immunoelectrode,

'n' is the number of electrons involved (usually considered unity, 1)

'A' is the sensing surface area, (0.25 cm^2)

'C' is the concentration of redox species, (5 mM $[Fe(CN)_6])^{3/4}$

'v' is the scan rate (50 mV/s).

The diffusion coefficient has been obtained to be **$5.1 \times 10^{-4} cm^2 s^{-1}$**.

The surface concentration of BSA/anti-CEA/PEDOT/RGO/ITO immunoelectrode has been estimated through **Brown-Anson** model

$$Ip = n^2F^2\gamma A\upsilon(4RT)^{-1} \text{ ……..……(viii)}$$

Where,

'I_p' is the peak current,

' A' is the surface area of the electrode,

'v' is the scan rate (V/s),

'γ' is the surface concentration of the absorbed electro-active species,

'F' is the Faraday constant (96485 C mol^{-1}),

'R' is the gas constant (8.314 J $mol^{-1}K^{-1}$) and

'T' is room temperature (25 ˚C or 298 K).

The surface concentration of BSA/anti-CEA/PEDOT/RGO/ITO immunoelectrode is estimated to be **$5.1 \times 10^{-11} mol\ cm^{-2}$**.

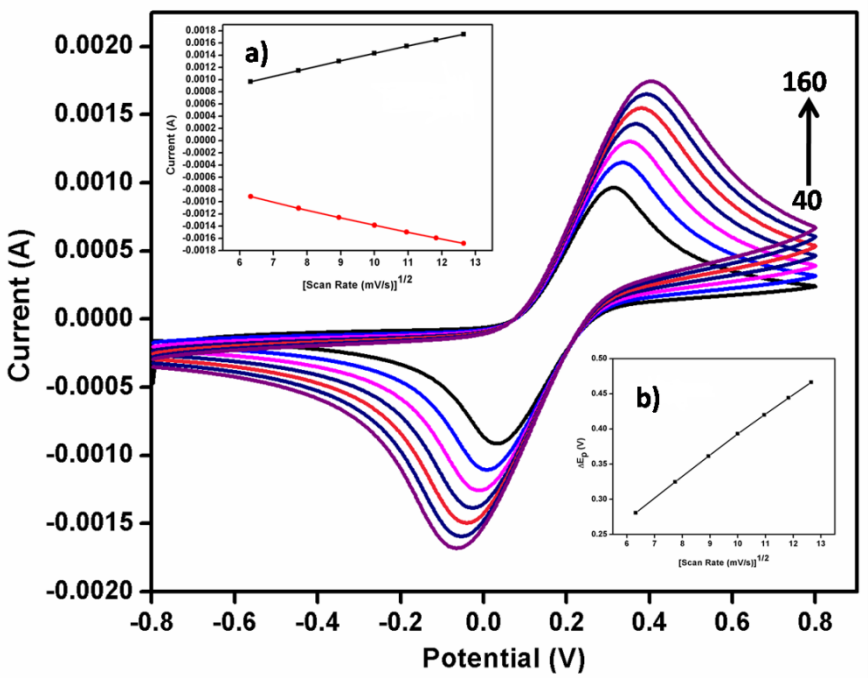

Figure 6. Cyclic voltammogram (CV) studies of PEDOT/RGO/ITO electrode as a function of scan rate (40-160mV/s), Inset (a) magnitude of oxidation and reduction current generated as response of scan rate (mV/s), Inset(b) potential as function of scan rate.

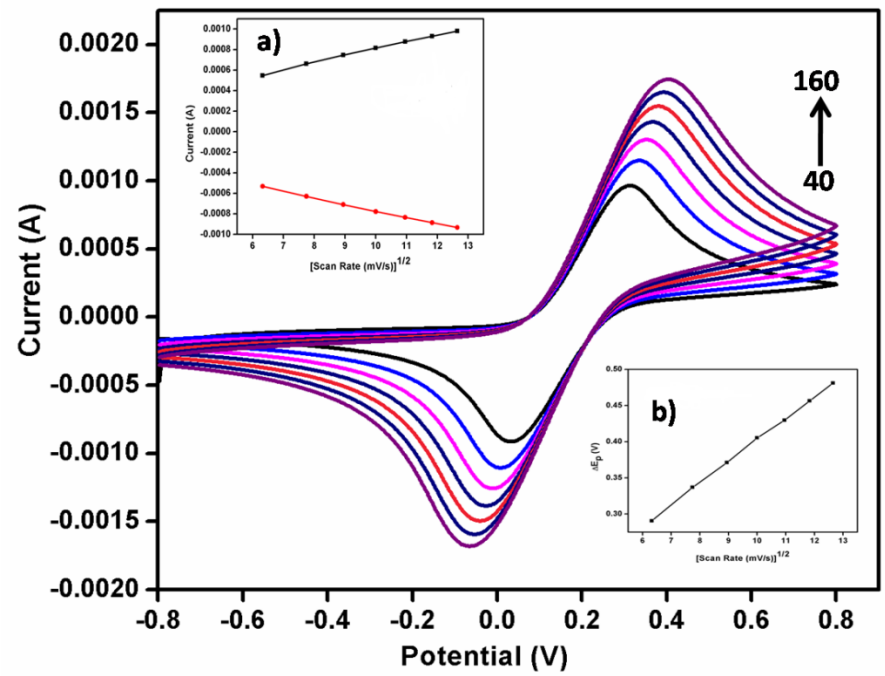

Figure 7.CV studies of BSA/anti-CEA/PEDOT/RGO/ITO immunoelectrode as a function of scan rate (40-160 mV/s), Inset (a) magnitude of oxidation and reduction current generated as response of scan rate (mV/s),Inset (b) potential as function of scan rate.

5.4 Electrochemical response studies

Differential pulse voltammetry (DPV) technique has been utilized to investigate the electrochemical response of the fabricated BSA/anti-CEA/PEDOT/RGO/ITO immunoelectrode as a function of anti-CEA concentration (0.50-15 ng mL^{-1}) in PBS buffer (50mM, 0.9% NaCl) containing $[Fe(CN)_6]^{3-/4-}$ (5mM). **Figure 8**shows DPV peak current of the immunoelectrode in the absence and presence of CEA antigen under optimized conditions. The response studies have been carried out in PBS (pH 7.0) containing 5mM $[Fe(CN)_6]^{3-/4-}$ in the potential range -0.4 to 0.6 V. The immunoelectrode is incubated with antigen solution for 15 minutes for antigen-antibody interaction prior to the DPV measurements. As seen in the figure, the peak current after the formation of antigen-antibody complex between CEA and anti-CEA decreased with increasing CEA concentration which was proportional to the CEA concentration in the range 0.50-15 ng mL^{-1}. The decreased current is attributed tithe formation of electrically insulating antigen-antibody complex that may obstruct the electron transfer through $[Fe(CN)_6]^{3-/4-}$ redox conversion. The obtained calibration curve between peak current and antigen concentrations obey the following linear equation (ix)

I_{pa}= [1.8 (μA mL ng^{-1}) × concentration of CEA (ng mL^{-1}) – 121 μA], R^2=0.981 …….(ix)

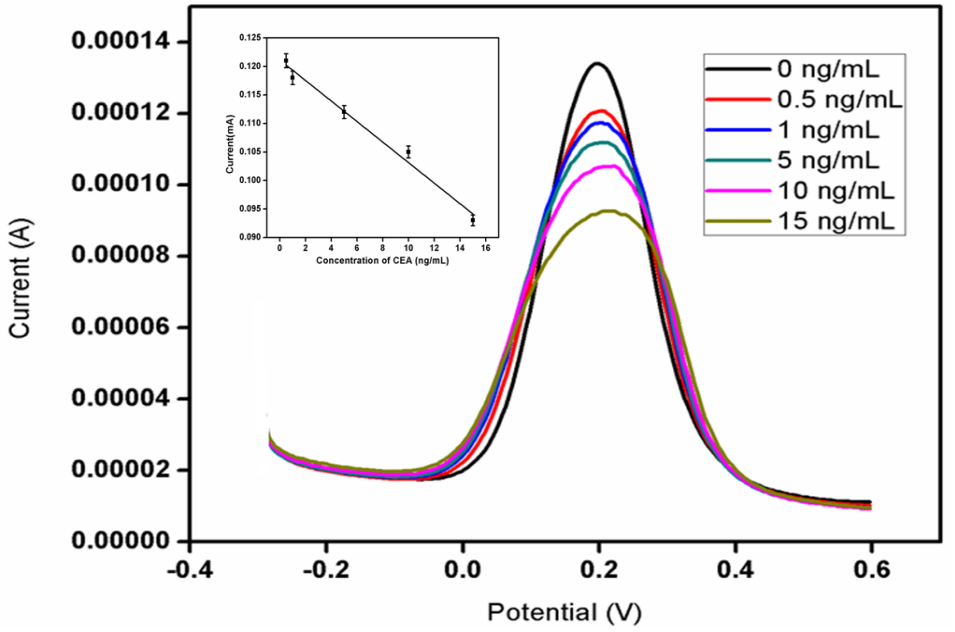

Figure 8. Electrochemical response of BSA/anti-CEA/PEDOT/RGO/ITO immunoelectrode as a function of CEA concentration (0.5 ng mL^{-1} to 15 ng mL^{-1}). Inset shows the concentration of CEA

Results of the electrochemical response in **figure 8 inset** studies indicate that the prepared BSA/anti-CEA/PEDOT/RGO/ITO immunoelectrode can be used to detect CEA in the range of **0.5–15 ng mL^{-1}** (R^2=0.98). The sensitivity of the fabricated immunoelectrode can be estimated by the slope of the curve and is found to be**1.8 µA mL ng^{-1}**. The standard deviation and limit of detection (LOD) for the immunoelectrode are obtained to be **12.49 x 10^{-5}** and **0.208 ng mL^{-1}**, respectively. The limit of detection has been calculated using the standard Equation (x):

Limit of detection = 3σ/Sensitivity…… (x)

Where,

'σ' is standard deviation of the BSA/anti-CEA/PEDOT/RGO/ITO immunoelectrode.

5.5 Control experiment

A control experiment was conducted using the PEDOT/RGO/ITO electrode under similar conditions **(Figure 9)**. We did not observe any significant change in the current response of the electrode with increasing concentration of CEA. These results reveal that PEDOT/RGO/ITO electrode does not interact with the antigen molecules in absence of antibodies.

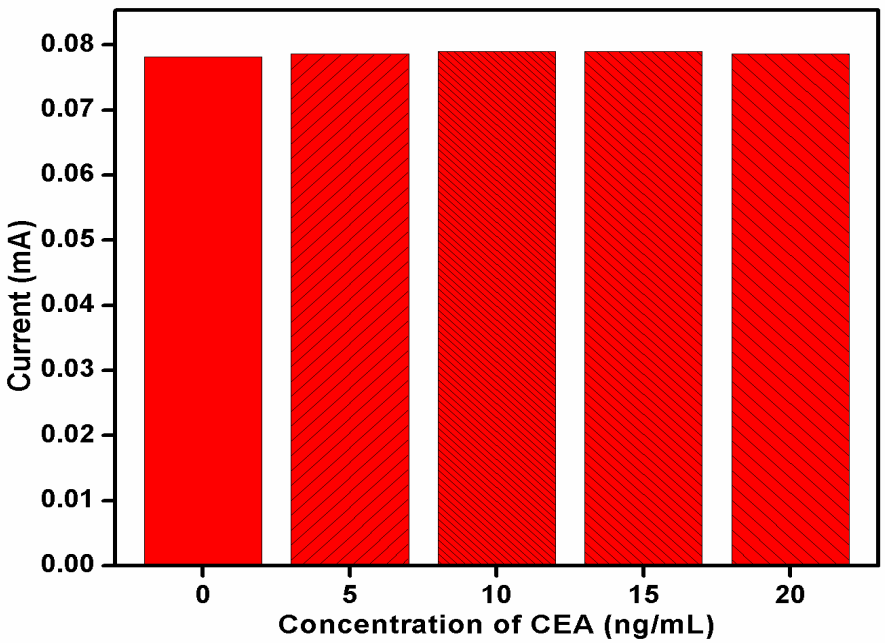

Figure 9.Control experiment (through electrochemical response study) of PEDOT/RGO/ITO electrode as a function of CEA concentration (0-20 ng mL^{-1}).

Chapter-6

Conclusions

The nanocomposite based platforms has shown to be excellent tools for diagnostics. In particular, their nature makes them available for POC applications, since they are portable and easy to use. Furthermore, the fast response is essential in many situations such as illness diagnostics which later require a fast treatment. The nanocomposite is expected to bring advances to their stability/robustness, shelf lifetime and bringing novel detection opportunities including multidetection capability besides other improvements of their analytical performance due to (i) large fraction of surface atoms; (ii)high surface energy; (iii) spatial confinement; (iv) reduced imperfections, which do not exist in the corresponding bulk materials that have been exploited to bring about a change in the diagnosis of a disease.

In conclusion, the protein functionalized PEDOT/RGO nanoparticles have been utilized for fabrication of a label free and efficient immunosensor for cancer detection. PEDOT/RGO nanoparticles have been synthesized via hydrothermal method. Thin films of PEDOT/RGO/ITO have been fabricated using electrophoretic deposition method that has been biofunctionalized with the anti-CEA antibodies. Results of the studies indicate that the fabricated BSA/anti-CEA/PEDOT/RGO/ITO immunoelectrode has good linearity, in the range, 0.5 to 15 ng mL^{-1} (with regression coefficient = 0.981), sensitivity of 1.8 μA mL ng^{-1} cm^{-2}, and lower detection limit of 0.208 ng mL^{-1}.Efforts should be made to utilize PEDOT/RGO based platform for detection of other cancer biomarkers.

Chapter-7

Future perspectives

The experimental investigations reveal that the PEDOT/RGO nanocomposite can be utilized in the development of high performance electrochemical biosensing devices with high sensitivity, selectivity, stability and design flexibility for laboratory applications.

Since the introduction of microfluidics technology in the early 1990s, an enormous amount of effort has been conducted towards the development of microfluidic immunosensors that combine the analytical power of microfluidic devices with the high specificity of antibody–antigen interactions. In the near future the nanocomposite (PEDOT/RGO; PANI/RGO; PEDOT/Iron oxide) based diagnostic nanobiosensors are expected to bring improvements in terms of sensitivity enhancement as well as the multiple molecules detection capability. In addition the most useful for their applicability as POC devices will be the possibility to communicate the results to specialized personnel. The major change expected in the future regarding diagnostics is hand held portable devices instead of the conventional bed side devices that rely heavily on trained personnel. The focus is on dummy proof devices those are user friendly and can be used at the comfort of one's home and give instant result. Nanobiosensors have the capability of revolutionizing diagnostics industry with improved sensitivity and analyte capturing. Due to surface modified with nanomaterials, the quantity of analyte required is minimal as the surface area for reaction is increased. Nanocomposite based nanobiosensors have gained momentum in the last decade and soon the market will flood with a number of such cost effective devices especially in the third world countries and developing nations.

Chapter-8

References

References

Ahuja, Tarushee, and Devendra Kumar."Recent progress in the development of nano-structured conducting polymers/nanocomposites for sensor applications." *Sensors and Actuators B: Chemical* 136.1 (2009): 275-286.

Alagarasi, A. "Introduction to nanomaterials." (2011).

Ali, M.A., Srivastava, S., Solanki, P.R., Reddy, V., Agrawal, V.V., Kim, C., John, R., Malhotra, B.D., 2013. Highly efficient bienzyme functionalized nanocomposite-based microfluidics biosensor platform for biomedical application. Scientific reports 3.

Arya, S.K., Bhansali, S., 2011. Lung cancer and its early detection using biomarker-based biosensors. Chemical reviews 111(11), 6783-6809.

Astruc, Didier, ed. *Nanoparticles and catalysis*.Vol. 1.Weinheim: Wiley-VCH, 2008.

Bae, Sukang, et al. "Roll-to-roll production of 30-inch graphene films for transparent electrodes." *Nature nanotechnology* 5.8 (2010): 574-578.

Balandin, A. A. Thermal properties of graphene and nanostructured carbon materials.Nature Mater.10, 569–581 (2011).

Banin Hirata B K, Oda J M M, LosiGuembarovski R, Ariza C B, Oliveira C E C d and Watanabe

Benchimol, Sarita, et al. "Carcinoembryonic antigen, a human tumor marker, functions as an intercellular adhesion molecule." *Cell* 57.2 (1989): 327-334.biosensors. *Biosensor and Bioelectronics* **17:345-349**

Bohunicky B and Mousa S A 2011 *Science and Applications* **4** 1-10

Cao, Guozhong. *Synthesis, Properties and Applications*.Imperial college press, London, 2004.

Che, Guangli, et al. "Metal-nanocluster-filled carbon nanotubes: catalytic properties and possible applications in electrochemical energy storage and production." *Langmuir* 15.3 (1999): 750-758.

Chen, JingHua, et al. "An ultrasensitive electrochemical biosensor for detection of DNA species related to oral cancer based on nuclease-assisted target recycling and amplification of DNAzyme." *Chemical Communications*47.28 (2011): 8004-8006.

De Palma M and Hanahan D 2012 *Mol. Oncol.***6** 111-27

Dey, S.R., Raj, C.R., 2010. J. Phys. Chem. C 114, 21427–21433.

Duffy, Michael J. "Carcinoembryonic antigen as a marker for colorectal cancer: is it clinically useful?." *Clinical chemistry* 47.4 (2001): 624-630.

Elliman, R. G., et al. "Optical emission from erbium-doped silica nanowires."*Journal of Applied Physics* 103.10 (2008): 104304.

Engelen, Mirjam JA, et al. "Serum CA 125, carcinoembryonic antigen, and CA 19-9 as tumor markers in borderline ovarian tumors." *Gynecologic oncology* 78.1 (2000): 16-20.

Faraday, M. "On the color of colloidal gold." *Phil. Trans. R. Soc. London* 147 (1857): 145-181.

Feng, Da-Qian, Guoliang Liu, and Wei Wang. "A novel biosensor for copper (ii) ions based on turn-on resonance light scattering of ssDNA templated silver nanoclusters." *Journal of Materials Chemistry B* 3.10 (2015): 2083-2088.

Feng, Lingyan, et al. "A graphene functionalized electrochemical aptasensor for selective label-free detection of cancer cells." *Biomaterials* 32.11 (2011): 2930-2937.

Feng, Xiaoping Han, and Shufeng Liu. "Development of an electrochemical DNA biosensor with a high sensitivity of fM by dendritic gold nanostructure modified electrode." *Biosensors and Bioelectronics* 26.5 (2011): 2619-2625.

Ferlay, Jacques, et al. "Cancer incidence and mortality worldwide: sources, methods and major patterns in GLOBOCAN 2012." *International journal of cancer* 136.5 (2015): E359-E386.

Flahaut, Emmanuel, et al. "Gram-scale CCVD synthesis of double-walled carbon nanotubes." *Chemical Communications* 12 (2003): 1442-1443.

Flanagan, Fidelma L., et al. "Utility of FDG-PET for investigating unexplained plasma CEA elevation in patients with colorectal cancer." *Annals of surgery*227.3 (1998): 319.

Galanis, Evanthia, et al. "Phase I trial of intraperitoneal administration of an oncolytic measles virus strain engineered to express carcinoembryonic antigen for recurrent ovarian cancer." *Cancer research* 70.3 (2010): 875-882.

Gerard M, Chaubey A, Malhotra BD **(2002)** Application of conducting polymers to

Gheith, Muhammed K., et al. "Stimulation of Neural Cells by Lateral Currents in Conductive Layer-by-Layer Films of Single-Walled Carbon Nanotubes."*Advanced Materials* 18.22 (2006): 2975-2979.

Gillette M A and Carr S A 2013 *Nat. Methods* **10** 28-34

Gold, Phil, and Samuel O. Freedman."Specific carcinoembryonic antigens of the human digestive system." *The Journal of experimental medicine* 122.3 (1965): 467-481.

Goldenberg, David M., et al. "Radioimmunodetection of cancer with radioactive antibodies to carcinoembryonic antigen." *Cancer Research* 40.8 Part 2 (1980): 2984-2992.

Goldenberg, David M., Robert M. Sharkey, and F. James Primus."Immunocytochemical detection of carcinoembryonic antigen in conventional histopathology specimens." *Cancer* 42.S3 (1978): 1546-1553.

Hammarström, Sten. "The carcinoembryonic antigen (CEA) family: structures, suggested functions and expression in normal and malignant tissues." *Seminars in cancer biology*.Vol. 9.No. 2.Academic Press, 1999.

Hanahan D and Weinberg Robert A 2011 *Cell* **144** 646-74

Hayes, Daniel F., V. R. Zurawski, and Donald W. Kufe. "Comparison of circulating CA15-3 and carcinoembryonic antigen levels in patients with breast cancer." *Journal of Clinical Oncology* 4.10 (1986): 1542-1550.

Henry N L and Hayes D F 2012 *Mol. Oncol.***6** 140-6

Herring, Conyers, and J. K. Galt."Elastic and plastic properties of very small metal specimens." *Physical Review* 85.6 (1952): 1060.

Heukelom, W., J. J. Broeder, and LL VANREIJEN. "* STRUCTURE ET TEXTURE DES CATALYSEURS NICKEL SUR SILICE DAPRES LES PROPRIETES FERROMAGNETIQUES." *JOURNAL DE CHIMIE PHYSIQUE ET DE PHYSICO-CHIMIE BIOLOGIQUE* 51.9 (1954): 474.

Hori S S and Gambhir S S 2011 *Sci. Transl. Med.* **3** 109ra16-ra16

Hurt E and Farrar W 2008 *MolInterv***8** 140 - 2

Ishigami, Sumiya, et al. "Clinical importance of preoperative carcinoembryonic antigen and carbohydrate antigen 19-9 levels in gastric cancer." *Journal of clinical gastroenterology* 32.1 (2001): 41-44.

Istamboulie, Georges, et al. "Screen-printed poly (3, 4-ethylenedioxythiophene)(PEDOT): A new electrochemical mediator for acetylcholinesterase-based biosensors." *Talanta* 82.3 (2010): 957-961.

Jin, Rongchao. "Quantum sized, thiolate-protected gold nanoclusters."*Nanoscale* 2.3 (2010): 343-362.

Jönsson, S. K. M., et al. "The effects of solvents on the morphology and sheet resistance in poly (3, 4-ethylenedioxythiophene)–polystyrenesulfonic acid (PEDOT–PSS) films." *Synthetic Metals* 139.1 (2003): 1-10.

Kang, X., Wang, J., Wu, H., Aksay, I.A., Liu, J., Lin, Y., 2009.Biosens.Bioelectron. 25, 901–905

Kim, W. H., et al. "Molecular organic light-emitting diodes using highly conducting polymers as anodes." *Applied Physics Letters* 80.20 (2002): 3844-3846.
Kroto, Harold W., et al. "C 60: buckminsterfullerene." *Nature* 318.6042 (1985): 162-163.

Kulpa, Jan, et al. "Carcinoembryonic antigen, squamous cell carcinoma antigen, CYFRA 21-1, and neuron-specific enolase in squamous cell lung cancer patients." *Clinical Chemistry* 48.11 (2002): 1931-1937.

Kumar, S., Kumar, S., Ali, M., Anand, P., Agrawal, V.V., John, R., Maji, S., Malhotra, B.D., 2013. Microfluidic-integrated biosensors: Prospects for point-of-care diagnostics. Biotechnology journal 8(11), 1267-1279.

Kumar, Saurabh, et al. "Reduced graphene oxide modified smart conducting paper for cancer biosensor." *Biosensors and Bioelectronics* 73 (2015): 114-122.

Lai, Ruay-Sheng, et al. "CYFRA 21-1 enzyme-linked immunosorbent assay: evaluation as a tumor marker in non-small cell lung cancer." *CHEST Journal*109.4 (1996): 995-1000.

Laurence, D. J. R., et al. "Role of plasma carcinoembryonic antigen in diagnosis of gastrointestinal, mammary, and bronchial carcinoma." *Br Med J*3.5827 (1972): 605-609.

Lee, C., Wei, X. D., Kysar, J. W. & Hone, J. Measurement of the elastic properties and intrinsic strength of monolayer graphene. Science 321, 385–388 (2008).

Li, Jing, et al. "Carbon nanotube sensors for gas and organic vapor detection." *Nano letters* 3.7 (2003): 929-933.

Li, Quanchang, et al. "Fabrication of ZnO nanorods and nanotubes in aqueous solutions." *Chemistry of Materials* 17.5 (2005): 1001-1006.

Liu, Chiu-Shong, et al. "Clinical impact of [18F] FDG-PET in patients with suspected recurrent breast cancer based on asymptomatically elevated tumor marker serum levels: a preliminary report." *Japanese journal of clinical oncology* 32.7 (2002): 244-247.

Lyuttsau, V. G., Yu M. Fishman, and I. L. Svetlov. "X-ray Study Of The Dislocation Structure Of Copper Whiskers." *SOVIET PHYS CRYSTALLOGR*10.6 (1966): 707-710.

M A E 2014 *Dis. Markers* **2014** 12

Madu C O and Lu Y 2010 *J. Cancer* **1** 150-77

Malhotra, Bansi D., Saurabh Srivastava, and Shine Augustine. "Biosensors for Food Toxin Detection: Carbon Nanotubes and Graphene." *MRS Proceedings*. Vol. 1725.Cambridge University Press, 2015.

Malhotra, R., Patel, V., Vaqué, J.P., Gutkind, J.S., Rusling, J.F., 2010. Ultrasensitive electrochemical immunosensor for oral cancer biomarker IL-6 using carbon nanotube forest electrodes and multilabel amplification.Analytical chemistry 82(8), 3118-3123.

Mehta S, Shelling A, Muthukaruppan A, Lasham A, Blenkiron C, Laking G and Print C 2010

Mie, G. "Articles on the optical characteristics of turbid tubes, especially colloidal metal solutions." *Ann. Phys* 25.3 (1908): 377-445.

Mody, Vicky V., et al. "Introduction to metallic nanoparticles." *Journal of Pharmacy and Bioallied Sciences* 2.4 (2010): 282.

Moertel, Charles G., et al. "An evaluation of the carcinoembryonic antigen (CEA) test for monitoring patients with resected colon cancer." *Jama* 270.8 (1993): 943-947.

Myers, Robert E., et al. "Carcinoembryonic antigen in breast cancer." *Cancer*42.S3 (1978): 1520-1526.

Nakane, Yasushi, et al. "Correlation of preoperative carcinoembryonic antigen levels and prognosis of gastric cancer patients." *Cancer* 73.11 (1994): 2703-2708.

Nakanishi, Hayao, et al. "Rapid quantitative detection of carcinoembryonic antigen–expressing free tumor cells in the peritoneal cavity of gastric-cancer patients with real-time RT-PCR on the lightcycler." *International journal of cancer* 89.5 (2000): 411-417.

Njagi, John, and Silvana Andreescu. "Stable enzyme biosensors based on chemically synthesized Au–polypyrrole nanocomposites." *Biosensors and Bioelectronics* 23.2 (2007): 168-175.

Nohara, Akira. "Effect of size on the strength of metal whiskers." *Japanese Journal of Applied Physics* 21.9R (1982): 1287.

Novak, J. P., et al. "Nerve agent detection using networks of single-walled carbon nanotubes." *Applied physics letters* 83.19 (2003): 4026-4028.

Pokropivny, V. V., and V. V. Skorokhod."Classification of nanostructures by dimensionality and concept of surface forms engineering in nanomaterial science." *Materials Science and Engineering: C* 27.5 (2007): 990-993.

Poole Jr, Charles P., and Frank J. Owens. *Introduction to nanotechnology*.John Wiley & Sons, 2003.

Preedy V R and Patel V B 2015 *Biomarkers in Cancer*: Springer

Rasooly, Avraham, and James Jacobson."Development of biosensors for cancer clinical testing." *Biosensors and Bioelectronics* 21.10 (2006): 1851-1858.

Ronning, C., et al. "Manganese-doped ZnO nanobelts for spintronics."*Applied Physics Letters* 84 (2004): 783-785.

Said, Jonathan W., et al. "Keratin proteins and carcinoembryonic antigen in lung carcinoma: an immunoperoxidase study of fifty-four cases, with ultrastructural correlations." *Human pathology* 14.1 (1983): 70-76.

Sherigara, Bailure S., WlodzimierzKutner, and Francis D'Souza."Electrocatalytic properties and sensor applications of fullerenes and carbon nanotubes." *Electroanalysis* 15.9 (2003): 753-772.

Shuster, J., Thomson, D. M. P., Fuks. A., and Gold, f? (1960). Immunologic approaches to the diagnosis of malignancy. Prog. Exp. Tumor Res. 25, 89-139.

Siqueira Jr, José R., et al. "Incorporating a hybrid urease-carbon nanotubes sensitive nanofilm on capacitive field-effect sensors for urea detection."*Analytical chemistry* 86.11 (2014): 5370-5375.

Solanki, P.R., Kaushik, A., Agrawal, V.V., Malhotra, B.D., 2011. Nanostructured metal oxide-based biosensors. NPG Asia Materials 3(1), 17-24.

Tartaj, Pedro, et al. "The preparation of magnetic nanoparticles for applications in biomedicine." *Journal of Physics D: Applied Physics* 36.13 (2003): R182.*Ther. Adv. Med. Oncol.* **2** 125-48

Thomson, D. M. P., et al. "The radioimmunoassay of circulating carcinoembryonic antigen of the human digestive system." *Proceedings of the National Academy of Sciences* 64.1 (1969): 161-167.

Tothill, Ibtisam E. "Biosensors for cancer markers diagnosis." *Seminars in cell & developmental biology*.Vol. 20.No. 1.Academic Press, 2009.

Vamvakaki, Vicky, Katerina Tsagaraki, and Nikos Chaniotakis."Carbon nanofiber-based glucose biosensor." *Analytical chemistry* 78.15 (2006): 5538-5542.

Voisin, C., et al. "Ultrafast electron-electron scattering and energy exchanges in noble-metal nanoparticles." *Physical Review B* 69.19 (2004): 195416.

Von Kleist, S., et al. "Immunohistology of the antigenic pattern of a continuous cell line from a human colon tumor." *Journal of the National Cancer Institute* 55.3 (1975): 555-560.

Wanebo, Harold J., et al. "Preoperative carcinoembryonic antigen level as a prognostic indicator in colorectal cancer." *New England Journal of Medicine*299.9 (1978): 448-451.

Wang, Joseph. "Amperometric biosensors for clinical and therapeutic drug monitoring: a review." *Journal of pharmaceutical and biomedical analysis*19.1 (1999): 47-53.

Wang, Joseph. "Electrochemical biosensors: towards point-of-care cancer diagnostics." *Biosensors and Bioelectronics* 21.10 (2006): 1887-1892.

Wang, Joseph. "Nanomaterial-based electrochemical biosensors." *Analyst*130.4 (2005): 421-426.

Wang, K., Ruan, J., Song, H., Zhang, J., Wo, Y., Guo, S., Cui, D., 2011b. Nanoscale Res. Lett.6, 8.

Wang, Z. L., et al. "Mechanical and electrostatic properties of carbon nanotubes and nanowires." *Materials Science and Engineering: C* 16.1 (2001): 3-10.

Wang, Z., Zhou, X., Boey, J.Z.F., Zhang, H., 2009c. J. Phys. Chem. C 113, 14071–14075

Wu L and Qu X 2015 *Chem. Soc. Rev.* **44** 2963-97

Xu, Dong, et al. "Quantitative real-time RT-PCR detection for CEA, CK20 and CK19 mRNA in peripheral blood of colorectal cancer patients." *Journal of Zhejiang University Science B* 7.6 (2006): 445-451.

Yonemura, Yutaka, et al. "Diagnostic value of preoperative RT-PCR-based screening method to detect carcinoembryonic antigen-expressing free cancer cells in the peritoneal cavity from patients with gastric cancer." *ANZ journal of surgery* 71.9 (2001): 521-528.

Zeng, Hailin, et al. "In situ polymerization approach to multiwalled carbon nanotubes-reinforced nylon 1010 composites: mechanical properties and crystallization behavior." *Polymer* 47.1 (2006): 113-122.

Zhang, Milin, et al. "Morphology-dependent redox and catalytic properties of CeO 2 nanostructures: nanowires, nanorods and nanoparticles." *Catalysis Today* 148.1 (2009): 179-183.

Zhang, Yingwei, et al. "A new preparation of Au nanoplates and their application for glucose sensing." *Biosensors and Bioelectronics* 28.1 (2011): 344-348.

Zhou, Feng, et al. "Sensitive sandwich ELISA based on a gold nanoparticle layer for cancer detection." *Analyst* 137.8 (2012): 1779-1784.